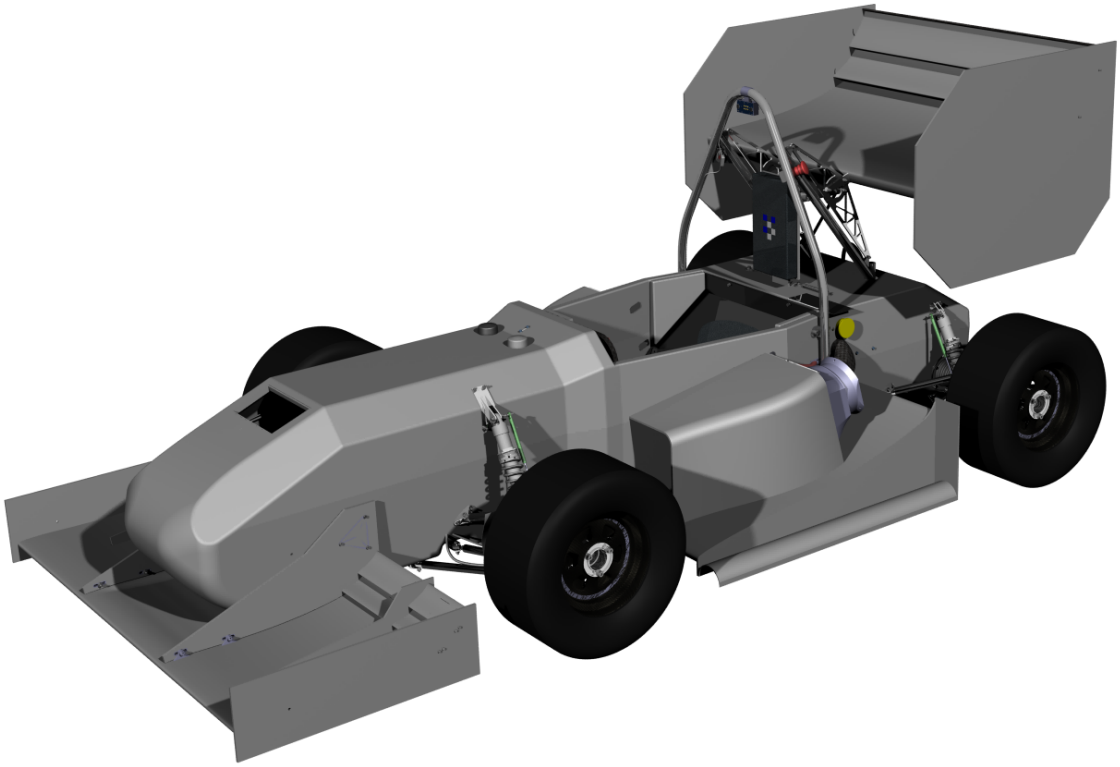

Active aerodynamics of an autonomous car

Master's thesis in Mechanics and Maritime Sciences

Samarth Malali Obaiah

Department of Mechanics and Maritime Sciences
CHALMERS UNIVERSITY OF TECHNOLOGY
Göteborg, Sweden 2023
www.chalmers.se

Master's thesis in Mechanics and Maritime Sciences

Active aerodynamics of an autonomous car

Samarth Malali Obaiah

CHALMERS
UNIVERSITY OF TECHNOLOGY

Department of Mechanics and Maritime Sciences
Division of Vehicle Engineering and Autonomous System
Chalmers University of Technology
Göteborg, Sweden 2023

Active aerodynamics of an autonomous car
Samarth Malali Obaiah

Supervisor: Ola Benderius, Department of Mechanics and Maritime Sciences
Examiner: Ola Benderius, Department of Mechanics and Maritime Sciences

Department of Mechanics and Maritime Sciences
Division of Vehicle Engineering and Autonomous Systems
Chalmers University of Technology
SE-412 96 Göteborg
Sweden
Telephone +46 31 772 1000

Printed by Chalmers Digitaltryck
Göteborg, Sweden 2023

Active aerodynamics of an autonomous car
Master's thesis in Mechanics and Maritime Sciences
Samarth Malali Obaiah
Department of Mechanics and Maritime Sciences
Formula student driverless
Chalmers University of Technology

ABSTRACT

Autonomous cars are one of the nascent technologies being focused on by many of the major automobile manufacturing companies. These new smarter cars allow for new possibilities in terms of integrated systems such as powertrain and safety. In the same way, manufacturers are trying to integrate vehicle aerodynamics into this smart ecosystem, making the car even more efficient and with improved performance. The first step towards smart aerodynamics can already be seen in present vehicles with features like active grille shutters, an extending tail section, and, in higher-end vehicles, the change in the angle of attack for the rear spoiler. The advantage of introducing smart aerodynamics into an autonomous Formula student car is very beneficial as the system already knows the path that the car is going to take. The basic function of the system is to feed the upcoming driving trajectory into the smart aerodynamics system, which in turn adjust aerodynamic character of the vehicle for example with help of wing profiles. As a result, the car will be ready to traverse the track in a more efficient manner.

The objective of this thesis is to develop a control system for the aerodynamics of the car to alter its track characteristics to best suit the needs of track topology and for other performance enhancements. Furthermore, the methods that are implemented to the car will is backed up with numerical simulation using fluid simulation software and validated through the results obtained.

Various techniques have been employed to enhance the aerodynamic characteristics with combinations of rear wing and front wing angle of attack manipulation. As a result, the improvements in terms of drag and lift are achieved.

Keywords: Autonomous car, Aerodynamic characteristics , Wing profiles, Numerical simulation, Fluid simulation, Drag and lift.

Acknowledgements

I take this opportunity to thank my supervisors, Prof. Ola Benderius and Dr. Alexey Vdovin, for giving me the chance to work on this exciting project in association with Formula student driverless. Their enthusiasm and exuberance have helped me to carry out my research with composure and confidence. Their guidance pushed me to think outside the box and helped me develop professionally as a student and as an engineer.
I also like to acknowledge my CFSD team as well. I learned more from them by their sheer commitment, passion, and eagerness to guide and teach a fellow teammate. Working with such a great team under great supervision has been more than a privilege, and I get humbled by it day by day.
Finally, I would like to thank my family and friends for always being there for me, especially my parents, who worked hard to get me here, get me a solid education, and help me to reach the position I always dreamed of. I want to thank all my professors and teachers for sharing their knowledge and experience to make me who I am today.

Samarth Malali Obaiah, Göteborg, 2023

Nomenclature:

Symbols

C_d	Coefficient of drag	[-]
C_l	Coefficient of lift	[-]
C_p	Center of pressure	[-]
C_g	Center of gravity	[-]
A	Frontal area	[m^2]
μ	Friction coefficient	[-]
$\mathbf{g}$	Gravity	[m/s^2]
F_{drag}	Aerodynamic drag force	[N]
F_{lift}	Aerodynamic lift force	[N]
V	Velocity	[m/s]
ρ	Density	[kg/m^3]
m_f	Front axle mass	[kg]
m_r	Rear axle mass	[kg]
∇	Gradient operator	[-]
dE	Change in energy	[J]
dW	Change in work done	[J]
dQ	Heat transferred	[J/K]
K_{us}	Understeer coefficient	[-]
β	Body slip angle	[rad]
ψ	Body yaw angle	[rad]
δ_f	Steering angle	[rad]
∇_p	Surface force	[N]
∇_r	Diffusion term	[-]

Abbreviations

AOA	Angle of attack
CAN	Controller area network
CFD	Computational fluid dynamics
CFSD	Chalmers Formula student driverless
CSV	Comma separated value
DNS	Direct numerical simulation
DRS	Drag reduction system
ECU	Engine control unit
IMU	Inertial measurement unit
PID	Proportional integral derivative
PWM	Power width modulation
LQR	Linear quadratic regulator
LES	Large eddy simulation
RANS	Reynolds average navier stokes

Contents

List of Figures

List of Tables

1
Introduction

A vehicle in motion is exposed to aerodynamic forces. These forces comes from the surrounding flowing air and will be the opposite to the vehicle's moving direction. Therefore, the vehicle will have to push through this resistance, resulting in power loss and affecting other performance factors. At the same time, this force can also be used to push the vehicle downwards, giving it good traction or road grip. Generally, a high-pressure force over the vehicle, and low pressure beneath it will generate a vacuum effect that helps to have a better grip on the road at higher speeds. Furthermore, these pressure forces proportionally increase with the square of the vehicle velocity. On the other hand, exerted pressure increases the drag of the vehicle as well, so the propulsion forces required to push the vehicle through this drag (resistance) also increase. In general, aerodynamics research aims to decrease this effect and improve the safety and overall performance of the vehicle.

1.1 Purpose

Aerodynamic forces are the dynamic loads that vehicles are exposed to during vehicle translatory motion, creating drag and lift on the chassis. The drag force acts opposite to the vehicle's moving direction and the lift force in the vertical direction, which adds to the downward forces exerted by the self mass of the vehicle [2]. Manipulating these aerodynamic force factors can bring substantial advantages to different driving scenarios. For example, considering a conventional on road vehicle, decreasing the vehicle's drag would improve fuel efficiency, making travel more environmentally friendly, and cost effective. The goal of a racing vehicle is different; it will be to achieve maximum traction at the expense of drag or positive lift.

1.2 Motivation

The purpose of the project connected to this thesis is to participate in racing competitions with the team of Chalmers Formula student driverless (CFSD). The goal of the thesis is to manipulate the aerodynamic downforce generated and to control it, also decreasing the negative impact of having a high downforce vehicle. The downforce will help the vehicle achieve good traction, making it possible to increase the speed over the chicanes. Overall, it improves acceleration and braking, and therefore may reduce the lap timing of the racing vehicle.

The developments of aerodynamics and computational fluid dynamics are highly driven by motorsports such as Formula One. Implementation of innovative technology is continuously encouraged to increase the vehicle's performance and decrease the lap timings. For current year's Formula student competition, the aero package illustrated in Figure 1.1 is used.

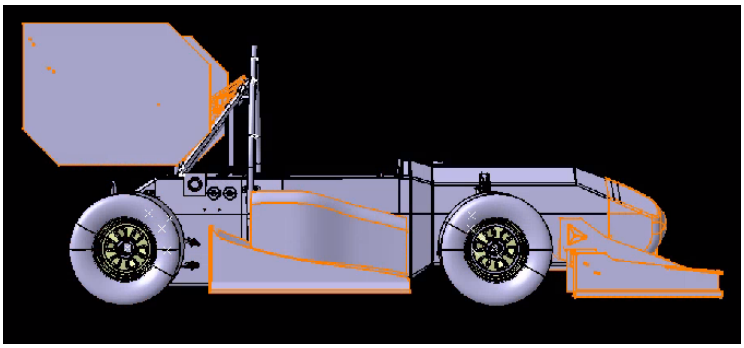

Figure 1.1: The CFSD21 car

The front section of the car houses multiwing elements. The sole purpose of this contraption is to create a negative lift (downforce) at the front, helping the car to get a better road grip while changing direction and during deceleration. The airflow over the front wing dictates the size of the rear wing profile as well as the passage flow over and underneath the car. In essence, the front wing dictates the aerodynamic performance of the car.

A diffuser was installed underneath the chassis providing the venturi effect (negative pressure aiding in the creation of suction), helping the vehicle stick to the road. The diffuser's venturi effect greatly depends on the front wing profile and the wake created by the wheels and suspension uprights.

The rear wing is one of the main sources of aerodynamic downforce generated in the vehicle, created by an upwash from the incoming flow resulting in the generation of downforce. In the current CFSD21 model, a high angle of attack wing is used. The wing generates more than 40% of the vehicle downforce, and works in conjunction with the front wing and diffuser to maintain a good aero balance.

When the individual sections of these aero packages are controlled or manipulated, the force acting on the chassis is altered and thereby changes the drag and negative lift. Manipulation of these aero packages can considerably improve the vehicle's performance.

Commercial on road vehicles have some basic concepts of active aerodynamics, such as active front fenders and extending spoilers. More advanced systems are implemented in some sports vehicles, which not only increases the performance of the vehicle, but also helps to achieve better road stability and fuel economy. Similarly, a CFSD car can also achieve better performance and road stability by adapting an active control system.

1.3 Challenges

There were certain factors that were challenging in the course of this project, such as modifications that had to be done to the mechanical hardware and the controller.

The main difficulty was to modify the current wing profiles and house a actuation process in the available space without affecting or changing other parts. This created a slight adverse effect on the air flow fed to the wings. Integration of new hardware and algorithms was required to govern those aero components without affecting the current system performance.

1.4 Research questions

This section lists the research questions that was addressed within the thesis.

- How is it possible to test the changes made to the aero package in simulation, and how is it possible to validate the results in a real environment?
- Using a fully developed active aero package in an autonomous racing vehicle, are there any improvements to its performance? Furthermore, what are the costs for such changes?
- What parts of the demonstrated active aero system could be adopted to benefit an autonomous passenger car?
- How much of a difference does the system make, comparing the active aerodynamics simulated in a computational fluid dynamics (CFD) environment to a real-world setting?

2

Background

According to Bernoulli's principle, an increase in the speed of a fluid or air occurs simultaneously with a reduction in static pressure [1]. In an inverted wing, the velocity of the flow will be high underneath the wing profile that generates the negative pressure, providing a downforce applied to the chassis of the vehicle. The downforce generated improves the traction in longitudinal and lateral travel directions. In turn, this improves the acceleration and deceleration of the vehicle. Doing so decreases the lift count and simultaneously increases the drag count [3]. The drag force is the frictional force, and that increases proportionally with speed. This increases the demand for power to overcome the resistance offered by the vehicle body to the incoming flow. Drag and lift are two important parameters to consider when designing the vehicle's aerodynamics. In general, drag and lift are interconnected. With the increase in downforce of the vehicle, the vehicle's drag also increases [4]. In this case, the drag is typically compensated for by obtaining a high downforce. Therefore, to determine the balance between the drag and lift, an efficiency factor is used. Aero efficiency defines how good of a balance there is between drag and lift or how much compensation is done with drag for getting a high downforce. Aero efficiency is a ratio of vertical force to the longitudinal force that defines how effective the vehicle aerodynamics. This can also be defined using a downforce coefficient (C_z along vertical direction), drag coefficient (C_x along longitudinal direction), and frontal area of the vehicle (A). Using these parameters will define the efficiency of the vehicle aerodynamics, like high efficiency and low efficiency design. For example, Formula One cars with high drag and high downforce (low efficiency design) will be quicker around corners, providing good traction. As a result, they will have slower lap timing than a low-drag and high downforce design (high efficiency design). The design requirements solely depend on the track layout and other parameters. For example, let us consider Formula One tracks like the Monaco street circuit track. Here, the vehicle's design requires high downforce as most of it is slow corners and chicanes. The Monza circuit is a high speed circuit, so the downforce requirement is less, and hence the drag of the vehicle will also be less. Therefore, the vehicle setup or design will always be a compromise between downforce and drag. Another term related to aerodynamics is the center of pressure (C_p) and center of gravity (C_g). The center of pressure is a point where the resultant forces of all aerodynamic forces are applied. This center of pressure point will be along the length of the vehicle's wheelbase. Through C_p position can determine the aerodynamic balance of the vehicle for example, if the pressure point is towards the front axle, then most of the downforce is being applied to the front wheel axle. If the pressure point is near the rear axle, then most of the downforce is applied to the rear axle. All the

parameters mentioned above can be interlinked through a term called aero balance.

Generally expressed as the downforce acting on the front wheels with respect to the whole aerodynamic forces acting on the car. Aero balance is given as the ratio of the product of the front axle downforce coefficient to the product of downforce coefficient of the whole vehicle ($\frac{C_{zf}}{C_z}$). By understanding the aero balance of a vehicle, one can predict how the vehicle will behave in corners. If the vehicle has more downforce towards the rear axle, then at fast corners the vehicle will experience an understeer as the rear axle is more loaded. Similarly, if the front axle has more downforce, it will have better grip at corners and less understeer, making it suitable for quick direction changes and braking.

There is one more factor that majorly contributes to the racing vehicle's aerodynamics, and that is the relative distance between the C_g and the C_p of a vehicle. For example, if C_p is behind C_g, then as the vehicle gains speed, the rear axle of the vehicle squats more. That will affect the venturi effect of the diffuser and thus decrease the downforce. If there is no suspension setup made to counteract this squat, and if C_p is in front of C_g, then the front axle squats as the speed increases. This parameter will be attributed to dynamic load distribution that indicates the relative forces acting on the front and rear axle [5].

Hence, from the early stages when the vehicle's aerodynamics started to improve, engineers began to address these issues relating to drag and the vehicle's overall shape. In the earlier stages of development, they reduced the vehicle's frontal area, in effect offering resistance to the vehicle's longitudinal motion. By reducing the frontal area, it not only reduced fuel consumption [6] also improved the ride dynamics and acoustics of road vehicles. The second step was redesigning the car structure from a box shape to curved, streamlined surfaces, which provides the least wind resistance. Doing so reduced the coefficient of drag of the car and significantly enhanced the aerodynamics efficiency of the vehicle. Most of the initial studies are done on a simple vehicle body (Ahmed body) to understand the flow around the body and the effects of drag and lift [7].

Through the recent conceptual design implementation, the aerodynamics of the vehicle significantly affected the performance and an active safety aspect. Adopted design systems were able to manipulate the road tire force interaction to enhance lateral and longitudinal safety [8]. The execution was not only for performance enhancement, it was also done from the point of active safety. The Formula One cars of 1966 were spotted with the first actual active moving components, where a rear wing *angle of attack* (AOA) was manually controlled by a driver through a pedal. This technique was used to increase downforce at corners by increasing the AOA of the wings. To reduce the downforce, the AOA is decreased, thus increasing straight-line speed [9]. Moreover, when it comes to high speed, the ground effect plays a significant role in road holding capability (creating a low pressure beneath the vehicle's underbody), and this can be achieved through manipulation of the diffuser [3]. In the coming years, electronics and sensors took over the control parts to actuate the system independently, efficiently, and safely. Initially, the idea of using movable flaps or wings was derived from the aviation industry. As we can see, aero carriers use aero governors such as wings and technical flow parameters to control the flying behavior as required and control it through either pilot intuition or a clever auto-

pilot system. The system monitors several parameters and decides the best course of action to actuate those wing elements. Later, this was carried over to on road vehicles. As a result, one can see that many race cars, supercars, and a few passenger cars are adapting active systems for aero vectoring to increase the efficiency, enhance ride quality, and enhance the safety of the vehicles [10]. Since an active aerodynamic system is well linked to riding comfort and with road holding capability, various studies and control oriented analysis and design experiments depending on several parameters have been investigated and proved the system adaptability [11].

The control strategy adopted by the active aerodynamics concluded that it would improve the lateral dynamics of the vehicle, or in other words, enhance the road handling capability and lateral stability [12]. An active rear wing spoiler will improve the lateral stability of the car over a sharp corner. Since its pitch is controllable, it will not decrease the performance of the vehicle in a longitudinal direction, this has been proved in simulation results and practical results [13]. To understand and estimate the handling behavior of the vehicle, linear models with n *degrees of freedom* (DOF) are used to accommodate all kinds of forces and moments in the system to make it as relatable to real world scenarios as possible. As the model's DOF increases, so does its complexity. Barari and his group have put a model and research paper to study handling behavior under aerodynamic forces [14].

In recent years, various control strategies have been considered for controlling the active aerodynamic surfaces or components, including *proportional integral derivative* (PID), *linear quadratic regulator* (LQR), and other controller methodologies to control active components [15]. The next step is arguably to implement this on a self-driving vehicle that uses vision technology and a machine learning methodology to adapt itself to the environment and is able to maneuver through the projected trajectory or upcoming path. Using this vision technology as a guidance system to other services such as battery monitoring, route planning, power deployment for the powertrain, or even the climatic control of the vehicle can be planned and controlled effectively. Using the same technique, the data from the projected path is fed to the aerodynamic system. By doing so, it can actuate the specific components of the aero package to adapt itself to the upcoming terrain or path by preparing the vehicle to behave or drive in a particular desired way. For example, if one consider a vehicle on a track with an autonomous system that has mapped the subsequent upcoming trajectory, now that data has been sent to the aero system, if the autonomous system has predicted a straight path, it can inform the aero system to decrease the drag or move the center of pressure accordingly. In other words, it will increase the vehicle's traveling velocity (if needed). Furthermore, the system can be programmed or trained to address a variety of other issues, such as braking and cornering in terms of oversteer or understeer. Integrating an autonomous system with the vehicle aerodynamics can impact the vehicle dynamics, making the whole system well connected and providing better controllability.

3
Theory

In this section, a concept for the changes to an existing car, to manipulate the drag force and downforce of the CFSD car. The conceptual idea was then verified with a *computational fluid dynamics* (CFD) simulation for the 1:1 CAD model of the car. A CFD analysis was conducted to analyze the lift to drag ratio generated according to the different setups.

3.1 Formulates for aerodynamics calculations

The equations that are going to be used for calculating the drag, lift, and moments in x (longitudinal) and z (vertical) directions acting on the vehicle are given below. It gives an idea of the forces and moments acting on the chassis of the vehicle.

$$C_d = \frac{2F_x}{\rho v^2 A} \tag{3.1}$$

$$C_l = \frac{2F_z}{\rho v^2 A} \tag{3.2}$$

$$C_{mx} = \frac{2M_x}{\rho v^2 AL} \tag{3.3}$$

$$C_{my} = \frac{2M_y}{\rho v^2 AL} \tag{3.4}$$

$$C_{mz} = \frac{2M_z}{\rho v^2 AL} \tag{3.5}$$

Where C_d is the drag coefficient, C_l is the lift coefficient, F_x and F_z are forces in longitudinal and vertical directions, ρ is the air density, v is the velocity of the vehicle, and A is the frontal area (direction dependent). Here, M_x, M_y and M_z are moments in a respective direction along the length of the body, which gives a good idea of the force vectors acting on the chassis for the respective wing and flap orientation.

3.2 CFD study

The Lynx is a *Chalmers Formula Student 17* (CFS17) car used for the purpose of this thesis. The race car was designed in Catia v5 and, with its simplification, carried over to a solver as a step file used in Star CCM+ for 3D CFD numerical analysis.

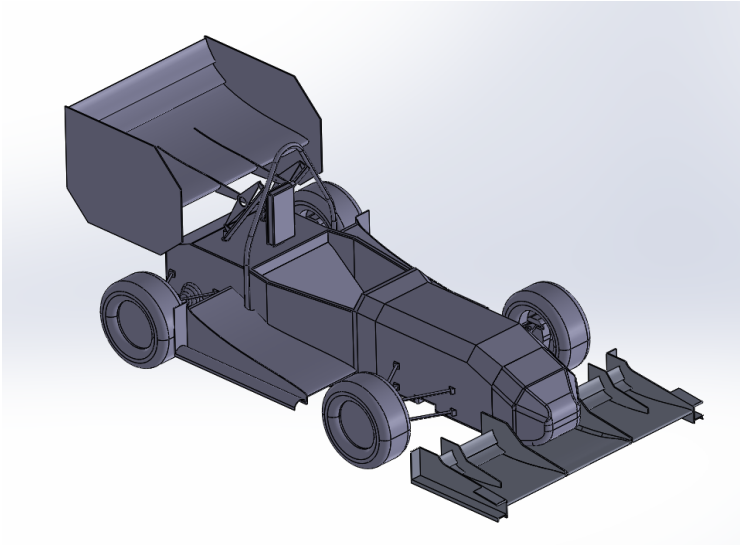

Figure 3.1: 1:1 scaled simplified model

3.2.1 Numerical modelling

Numerical modelling helps us to understand the flow behavior by quantifying it with a partial differential equation and representing it with the law of conservation of mass, momentum, and energy. CFD is a branch of fluid dynamics that utilizes numerical analysis and algorithms to solve fluid flow solutions [18].

The Navier Stokes equation is the most commonly used primary method of solver used in CFD software. The Navier Stokes equation is an extension of Newton's second law of motion for fluids by correlating with the stress in the fluid and is the sum of a diffusing viscous term and the pressure term. What these equations try to describe is how the pressure, velocity, density, and temperature of moving fluid change over time and direction [19].

As mentioned previously, three basic governing equations give a basic structure for thermo fluids, and these are based on the conservation law of fluid physics properties;

- Conservation of mass: Continuity equation
- Conservation of momentum: Newton's second law
- Conservation of energy: Energy equation

To understand or to estimate the fluid flow, we need to know the velocity, pressure, and temperature throughout every point of the flow regime. Kinematic properties

and movements of a fluid can be investigated either through Lagrangian or Eulerian methods.

If expressed through equations, it will be with respect to coordinates:

Langragian flow: study of a particular single fluid particle, where we observe its change in its properties such as velocity, acceleration, and density.

$$x = x(a, b, c, t) \;\; y = y(a, b, c, t) \;\; z = z(a, b, c, t)$$

where a, b, and c are coordinates of the particles and x, y, and z are coordinates of the same particle with respect to time.

Eulerian flow: Fluid particle study at a specific region or fixed point will observe variations in velocity, acceleration, and density at that specific fixed point.

$$u = u(x, y, z, t) \;\; v = v(x, y, z, t) \;\; w = w(x, y, z, t)$$

where u, v and w are velocity of particles at points (x, y, z) respective to time t.

Understanding the fundamental conservation equations:

1. Conservation of mass: Continuity equation is given as

$$\frac{D\rho}{Dt} + \rho(\nabla \overrightarrow{v}) = 0 \tag{3.6}$$

where ρ is density, ∇ is gradient operator and $\overrightarrow{v}$ is velocity vector.
Above expression can be explained as "The rate of change of mass inside a control volume must be equal to the volume of fluid entering that volume." [20]

2. Conservation of momentum: also know as Navier Stokes equation

$$\frac{\partial}{\partial t}(\rho \overrightarrow{v}) + \nabla(\rho \overrightarrow{v}) = -\nabla p + \nabla \tau + \rho \overrightarrow{g} \tag{3.7}$$

where p is static pressure, τ is stress tensor and $\rho \overrightarrow{g}$ is force per unit volume. Moreover, the whole equation can be divided into five segments to understand the significance of each,

- $\frac{\partial}{\partial t}(\rho \overrightarrow{v})$ is Local change with time.
- $\nabla(\rho \overrightarrow{v})$ is Momentum convection.
- ∇p is Surface force.
- $\nabla \tau$ is Diffusion term.

- $\rho \overrightarrow{g}$ is mass force.

The above expression can be explained as "Any change in momentum of the fluid within the control volume will be due to the net flow of momentum into the volume and the action of external forces acting on the fluid within the volume." [20]

3. Conservation of Energy: Energy equation is given as:

$$dE_t = dQ + dW \tag{3.8}$$

where dW is work done on the system, dQ is the heat added to the system, and dE_t is the increment in the total energy of the system.

Newtonian fluid (the viscous force or deformation acting on fluid results in stress on fluid which is linearly related to strain) like air and water. Making it simple to numerically understand and simulate the above three conservation's over the medium. Next is the fluid state, turbulent or laminar. Turbulent flow is characterized by recirculation, smaller eddies, and random chaotic patterns, distributing or losing momentum, energy, or temperature through these characteristics. The laminar flow will be the flow with a constant linear non chaotic pattern. The Reynolds number can be used to establish these fluid flow properties, which aids in distinguishing and comprehending them. The Navier Stokes equations can be used to describe the turbulent flow and simulate its behaviour. The higher the Reynolds number, the greater the computational burden and it requires a higher computational system to simulate it.

There are numerous turbulence models to compute the physical property changes over the medium due to turbulence and particle-medium interaction. As for naming a few models, such as

- DNS : Direct numerical simulation
- LES : Large eddy simulation
- RANS : Reynolds averaged navier stokes
- K-ϵ : k Epsilon model
- k-ω : k Omega model
- SST : Shear stress transport model

The next step is the analysis of the fluid and steps for mesh generation. The partial differential equation is used to govern the fluid flow. To analyze the fluid flow, domains are used, such as hexahedral and tetrahedral in the 3D domain and for the 2D domain with quadrilaterals and triangles. Then these confined places are used to discretize and solve within these domains. These domains are called cells or elements, and the collection of cells is called a mesh or grids. Developing these meshes is as important as choosing a suitable model for computation, as these

grids dictate how well the whole domain is segregated and how partial differential equations can be solved individually in the respective cells [21].

The transfer of energy in CFD simulation is analyzed using grids from one cubical grid to the next. As the flow moves, the energy is passed on. There are multiple models used to predict these transfer functions, each model is suitable for particular models, methodologies, and accuracy level. In this project, the k epsilon model is a suitable choice in terms of accuracy, convergence rate, and computational power required. However, meshing around the vehicle to understand the flow grid division over the whole vehicle structure also needs to be considered. Eventually, a wall treatment model has to be included near the surface of the vehicle to estimate the flow turbulence and character of the flow near the surface. Enlarge the mesh size everywhere else with this technique. It can reduce the computational requirements and time [16].

Post processing is the method of visualizing the computational fluid dynamics data and helps us derive an accurate conclusion from the models. Post results may include graphs, plots, scalar scenes, and streamlines over the medium that help to understand the flow's behaviour over the surface of the medium as intended or as modeled. The results shown from these methods verify how good our chosen solver, mesh quality, and complete model are. From this data, we can corelate with real life flow characteristics (which can be visualized using tufts or flowvis on a live medium) to compare and validate the simulation results and iterate if they requires any modification.

3.3 Control theory

This section will discuss the actuation method and process involved in controlling the movements of multiple elements of the wing. And the reason behind this actuation is how it links vehicle dynamics and aerodynamics.

3.3.1 Control philosophy

Generally, when the vehicle is moving, the vehicle will undergo dynamic load distribution across the length of the vehicle. Since wheels are the transient medium between the chassis and the road, one can see the vehicle's behavior through the force transmitted from the wheels to suspensions. By the squat, dive, and heave of the vehicle chassis, one can estimate which axle and wheels most of the forces are acted upon.

From Figure 3.2, the vehicle will have a different kind of motion and rotation on each axis. Totally, there are around six degrees of freedom to define vehicle's translation movements.

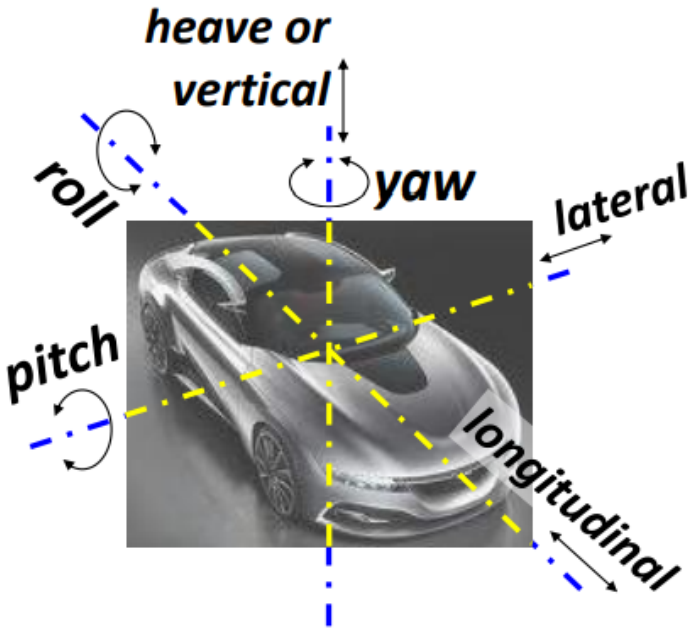

Figure 3.2: Vehicle degrees of freedom (image courtesy [22]

The friction circle or traction circle is as shown in Figure 3.3. Every tire has a limited amount of traction or grip depending on its compound or friction coefficient (μ). Within this limit, the tire will give optimum traction for requested action, either longitudinal travel (forward motion: acceleration and braking) or lateral travel (steering action or cornering). The friction circle can be depicted by knowing the tire's friction coefficient (μ), vehicle mass (mass in vertical direction F_Z), and road's friction coefficient (μ_r).

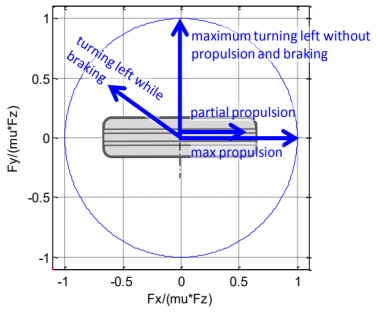

Figure 3.3: The friction circle (image courtesy [22])

During cornering, the vehicle undergoes a centrifugal reaction to the motion and rolls in the opposite to direction of cornering. Consequently, it translates most of the vehicle's body mass onto the outside wheels. This rolling results in the outer wheel being more loaded than the inner wheel, limiting the traction provided by the inside

wheels, which is paramount while turning, as it helps to grip the inner radius of the road better and helps to turn quicker. As the speed increases while cornering, the lateral acceleration of the car also increases, as does the weight transfer. If the outside wheels reach there traction limit or outside of its friction circle, then the vehicle either over steers or under steers, making the vehicle trajectory unpredictable.

During cornering, the response of the vehicle depends on characteristics such as speed and road surface. The vehicle may undergo neutral, under, or over steered due to the limit of friction. Neutral steer is when the friction provided by the wheels is sufficient to undergo the requested maneuver without a change in behaviour of the vehicle. Understeer is when in a corner, the vehicle tends to go in a straight line and requires more steering input. Oversteer is when the vehicle's rear end spins more than needed and requires counter-steering action. A formulation for the understeer coefficient (K_{us}) helps to explain this behavior.

$$K_{us} = \frac{m_f}{c_{\alpha f}} - \frac{m_r}{c_{\alpha r}} \tag{3.9}$$

where m_f and m_r are the load on each axle/tire and $c_{\alpha f}$ and $c_{\alpha r}$ are tire cornering stiffness for both front and rear tires respectively.

- If $K_{us} = 0$. Then vehicle is undergoing neutral steering, which means the slip angle of the front (α_f) and rear (α_r) tire or axle are equal.
- If $K_{us} > 0$, Then the vehicle is undergoing understeer, which means the slip angle of the front tire/axle is more than the slip angle of the rear tire or axle.
- If $K_{us} < 0$. Then the vehicle is undergoing oversteer, which means the slip angle of the front tire/axle is less than the slip angle of the rear tire or axle.

Usually, the above phenomenon will be counteracted by an *electronic stability program* (ESP). For an understeered vehicle, the ESP system will brake the inner rear wheel, creating momentum to rectify it. In the event of oversteering, the ESP system will brake the outer front wheel. By doing so, it will straighten the momentum of the vehicle.

Body slip angle (β) and yaw rate (Ψ) are two vital parameters to determine the stability of the vehicle and the way to control it. Body slip angle can be calculated by knowing the longitudinal and lateral speed of the car.

$$\beta = tan^{-1}\frac{v_x}{v_y} \tag{3.10}$$

Similarly, for formulating the yaw rate (Ψ) requires vehicle speed (v), understeer coefficient (K_{us}), steering angle (δ_f), wheel base (L) and gravity (g).

$$\Psi = \frac{v}{L + K_{us}v^2/g}\delta f \tag{3.11}$$

By monitoring and regulating β and Ψ one can understand and control the vehicle's stability. ESP calculates the deviation in the above parameters and initiates the necessary corrective action to keep the vehicle stable.

Therefore, for the stability control system to work as intended, various sensors can be employed in the vehicle like,

- Wheel speed sensor at each wheels
- Brake sensors at each wheels
- Steering wheel angle sensor
- Yaw and acceleration sensor
- Engine control management (ECU)
- Temperature sensor
- Damper position sensor on each suspension uprights

The damper position sensor (linear movement positioning sensor), which is adapted to each suspension, provides information about the dynamic loading on each wheel. A gyroscopic instrument can be used to know the relative position, velocity, and acceleration of a vehicle with respect to the ground in a longitudinal and lateral direction. An *inertial measurement unit* (IMU) can be used to determine the longitudinal acceleration (a_x), lateral acceleration (a_y) and yaw rate of the vehicle. The mentioned sensors are used as input for the algorithm to detect and predict the vehicle's movement and estimate how the vehicle is behaving.

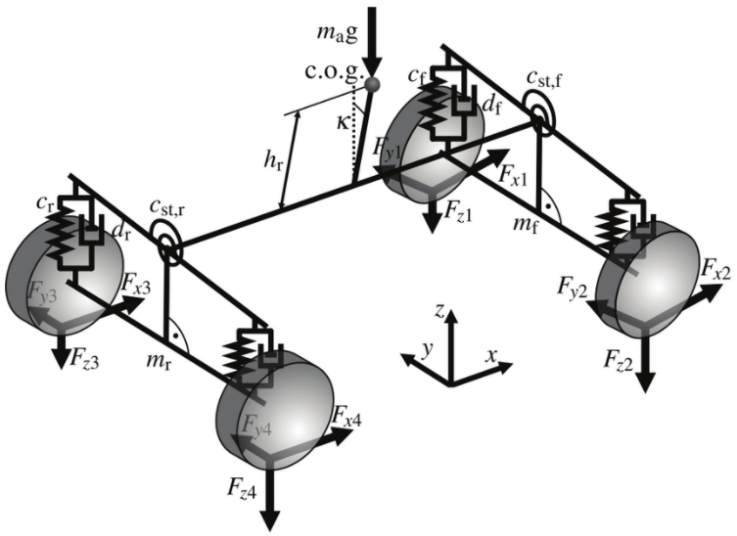

Figure 3.4: Forces on front and rear axle (image courtesy [22])

Like the ESP system, instead of using brakes and the engine as a source of rectifying action, one can use aerodynamic forces to balance or stabilize the vehicle's

lateral action. In general, wings provide the required downforce on to the chassis, which adds on top of the vertical mass (F_z) of the vehicle.

$$F_{ztot} = F_z + F_{zair} \tag{3.12}$$

The additional vertical mass provides good traction for the tire by enlarging the contact patch. However, when the vehicle yaws or rotates, the downforce created deviates as well. By controlling the downforce created on each side of the wing, one can change the vertical force on individual wheels, such as the rear right (F_{z1}), rear left (F_{z2}), front right (F_{z3}), and front left (F_{z4}), as shown in Figure.

The downforce created by the aero package is advantageous when requiring as much traction as possible, that is, when the flaps in the wings are in the closed or high AOA position. However, the downside of this setup is that the drag created by the high AOA compensates for the propulsion forces required to punch through the air, resulting in a loss of power and low speed. As a result, the goal is to reduce drag in the straight line, which will allow the car to gain momentum. In that case, active aero is a fundamental concept of a *drag reduction system* (DRS) of Formula One motorsport, where the driver needs to manually activate DRS when the driver is in a specific area with a specified relative distance/time with another car in front. Usually, the actuation of DRS will be on the straight part of the track. This will reduce the drag and increase the vehicle's overall speed by decreasing the vertical force created by the wing on the chassis. Now the total vertical force on the chassis will be mostly from the mass of the vehicle.

$$F_{ztot} = F_z + \cancel{F_{zair}}^{zero} \tag{3.13}$$

From Figure 3.5, one can see the DRS activation on particular parts of the circuit.

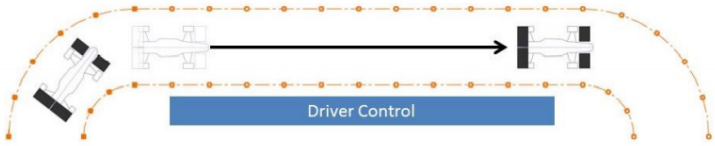

Figure 3.5: DRS activation zone

Meanwhile, in corners, traction on the wheels is required, which will help for quick direction changes and allows to take more speed into the corner and getting out of the corner at a better speed and racing line. To achieve a proper vehicle alignment without any undesired characteristics such as understeer and oversteer. To achieve this, the front wing plays a significant role in front wheel traction by increasing the downforce and increasing the front tire contact patches. Front wing

elements will help to distribute the forces between the wheels of the front axle. The CFS17 car has a multi element front wing section, where each side wing element will be activated independently of one another. When the vehicle is taking a turn, the outer wheels will be loaded more due to centrifugal force, shifting the vehicle's balance from an equally distributed mass to the majority of the mass shifted to the outer wheels. Because of that, the inner wheels will have less traction compared to the outer wheels. The control strategy in this situation will be to reduce the downforce on the outer wheels and increase the downforce on the inner wheels. This will help to distribute the vertical forces almost equally among the four wheels.

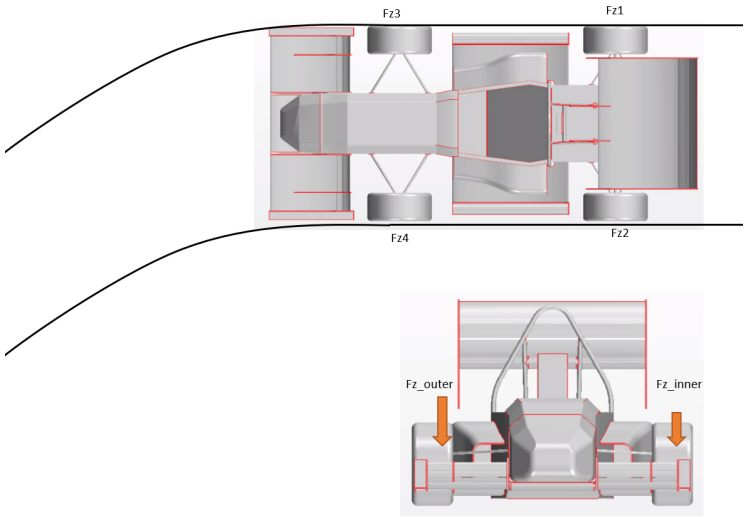

Figure 3.6: Forces while cornering

Thus, the objective of the system is to distribute the vertical aerodynamic forces equally on each wheel. Therefore, it provides sufficient grip and traction for the tires to work in optimum traction conditions. The functionality of the control system and its pre-requisites are explained in the next section.

4
Method

To understand the flow around the Formula Student car and to validate the changes employed in a numerical sense. The initial step is to build a 1:1 scale model in a CAD tool, subsequently importing that model to a simulation environment to prepare it for simulation. In the following steps, the design process and CFD software implementation are discussed.

4.1 CAD model

Figure 4.1 shows CFS 17 car, as this is the same car we are currently modifying to be driverless. Dimensionally, it is as close as possible to the original car. The only assumptions are that finer details like suspension uprights and wheel components, such as brake discs and calipers, are omitted in the final design, as this will reduce complexity while meshing and increases the computational time when imported to the CFD software. Moreover, assuming these minor geometry changes are unlikely to make that much of a difference in the simulation results. Apart from these two modifications, every other design aspect of the car will be kept true to the real car. The wheel section is a fully covered unit and have an axis point to mimic its rotation while moving, as it is one of the significant sources of wake in the vehicles. Most of the CAD modeling was done using Catia V5. The Figure 4.1 shows the overall dimensions of the car:

4.2 CFD modelling

This section will briefly explain the CFD analysis performed on the 1:1 CAD model. The Star CCM+ software was used for meshing, analysis, and post processing. The work involved defining the model parts, splitting them into patches, and naming them according to the specifications. Additionally, the flow domain was modeled to match the real world conditions and to avoid any blockage or development of wake in the nearby region, so that it would not affect the flow in any way. To reduce the computational effort and time, the model was divided in the middle (along the track width), creating symmetry on both sides. In this way, the simulation was conducted over half of the vehicle's surface, thus reducing cell counts and computational costs. The meshing method, coordinates, and physical models used are briefly explained below.

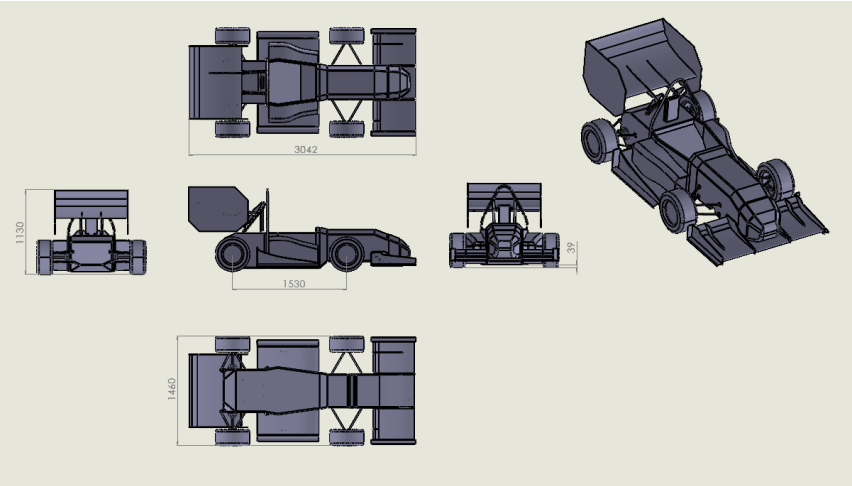

Figure 4.1: CAD model with overall dimensions

4.2.1 Coordinate system

The coordinates followed in the model are; along x direction is along the vehicle wheelbase, along y direction is the track-width of the vehicle, and z is along the height of the vehicle. The model was placed in the computational domain, with the vehicle facing the flow from the input side. A symmetry plane was established upon which a vehicle is divided into two sections, as previously explained, to reduce the number of cells. The frontal area of the vehicle is around $1.06\,\mathrm{m}^2$ along the x direction. Figure 4.2 shows the placement and direction of the vehicle model in a domain.

4.2.2 Computational domain and meshing

The computational domain is a domain that acts as a real world environment for the object of interest placed inside it. It can simulate the airflow of a real world scenario and resemble the full scale wind tunnel, which can help when analyzing and understanding the flow around the vehicle. As per best practice, the total size of the domain plays a significant role in developing a flow and making sure it does not have any blockage effect. Hence, the domain dimensions are followed in a general sense. The total length of the domain is thirteen times the length of the vehicle, the height of the domain is six times the height of the vehicle, and the width of the domain is seven times the wheelbase of the vehicle. To create a tire patch, the wheels are submerged into the ground with a dimension of 0.31 m in the negative z direction. The vehicle is placed exactly 11.7 m offset from the input of the wind tunnel domain. Figure 4.2 and Table 4.1 give the exact dimensions of the domain.

Meshing the vehicle was modeled and assembled in Catia V5 and then imported to Star CCM+ as a step file with medium tessellation. The first step was then to surface wrap the whole vehicle surface to cover any holes or gaps. Surface wrap

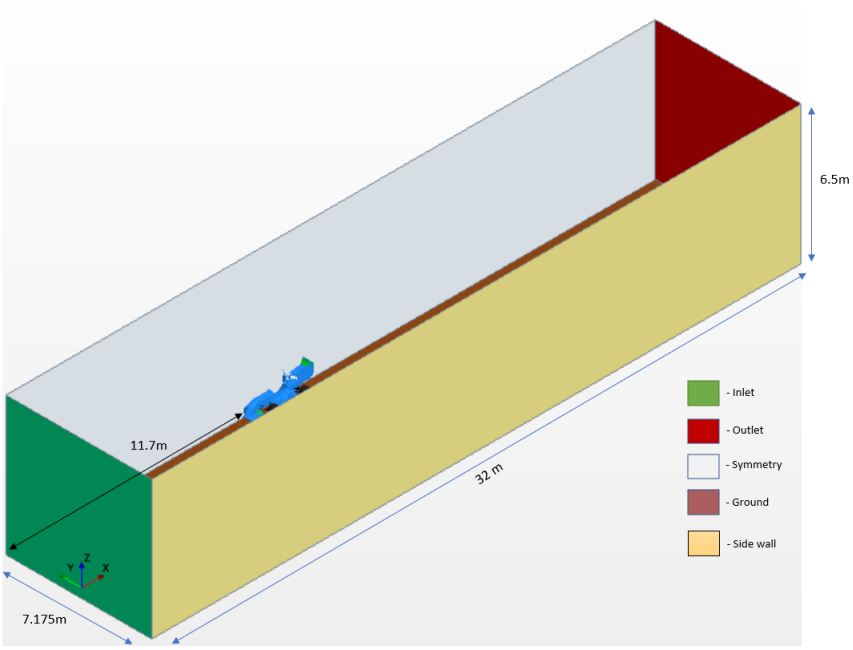

Figure 4.2: Wind-tunnel layout in the simulation

Windtunnel domain	
Length	32 m
Width	7.175 m
Height	6.5 m

Table 4.1: Domain dimensions

with a base size of 0.02 m was implemented for closing minute gaps, covering intricate shapes and curvatures. Then the surface wrapped geometry was subtracted from the windtunnel domain. Meshing the rest of the subtracted geometry with an automated mesh, with meshing models such as surface remesher, automatic surface repair, polyhedral mesher, and prism layer mesh. In these models, the first two are for surface operations and the last two are for volumetric operations.

Surface meshing is to redefine the surface mesh over the entire region, a surface remesher is used. It divides the whole domain into boundaries with the smallest cell size and the largest cell size, emphasizing the simulation's accuracy and computational cost. To achieve this, each region is refined with regard to its wake region and with a slow surface growth rate, thus providing a smooth transition between cells of different sizes. For example, from Figure 4.3, one can distinguish between the sizes of cells in two parts (front cone and front wing), aiming to capture the flow accurately. Moreover, the feature of automatic surface repair rectifies the generated surface mesh if there is any contradiction between the given dimension and edge feature, which helps to keep the cell quality above a required threshold value.

Volumetric meshing, Polyhedral cells are the most commonly used meshing models. Due to the ease of mesh generation for complex shapes, it combines the

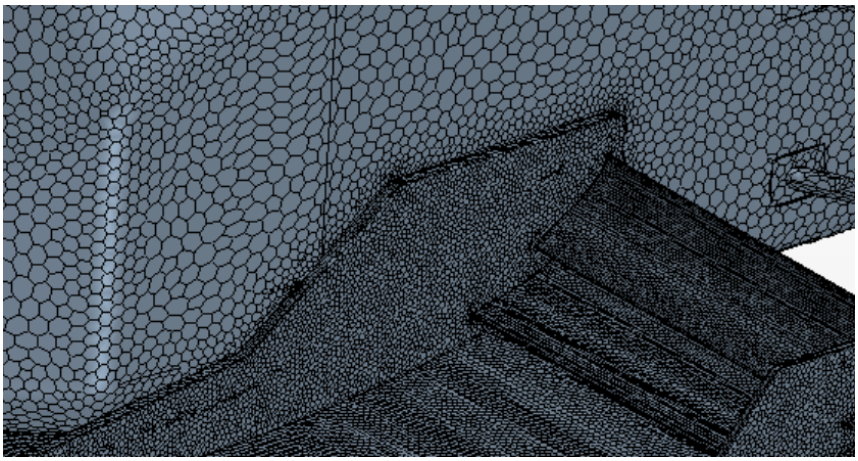

Figure 4.3: Cell size comparison between the front wing and monocoque

best of hexahedral and tetrahedral in terms of accuracy and rapid mesh generation. Since the current region has numerous neighbor cells, it will help in accounting for gradient changes. For the current model, many layers of refinement in terms of cell volume have been implemented. As a result, it can capture finer details of airflow characteristics near the object of interest and at the same time maintain consistency away from the object of interest. Figures 4.4 to 4.6 represent the domain meshing methodology followed to resolve the flow physics and wake as accurately as possible.

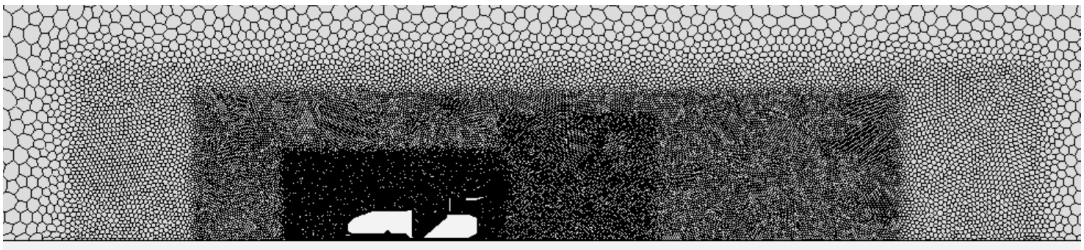

Figure 4.4: Meshing domain: Side view

Prism layers is the prismatic cells on the walls are for boundary flow accuracy. As air flows over a surface, there will be a boundary layer formed over it, which is directly dependent on Reynolds number, flow velocity, and material properties. Prism layers are used to capture the boundary layer formed over the surface. The boundary layer formation over the vehicle's surface and on the ground or road creates a relative velocity between free stream velocity and the boundary layer. Hence, the wall treatment model or wall law is defined as "The average velocity of turbulent flow at the free stream velocity point is proportional to the logarithmic of the distance from the wall to that point"[21]. The y^+ value defines the distance between the wall and the free stream velocity point. This is a non dimensional number used to describe the boundary layer for turbulence modeling. y^+ is calculated as

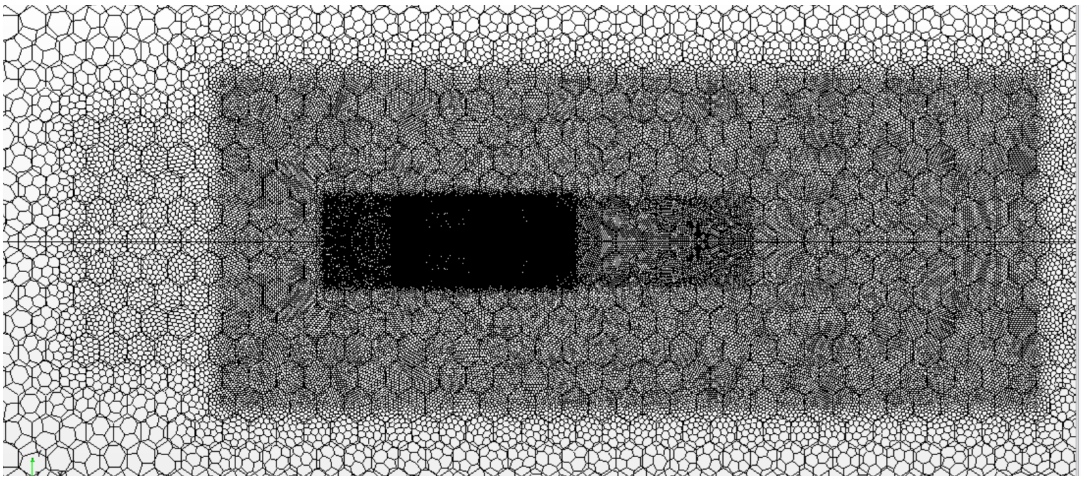

Figure 4.5: Meshing domain: Top view

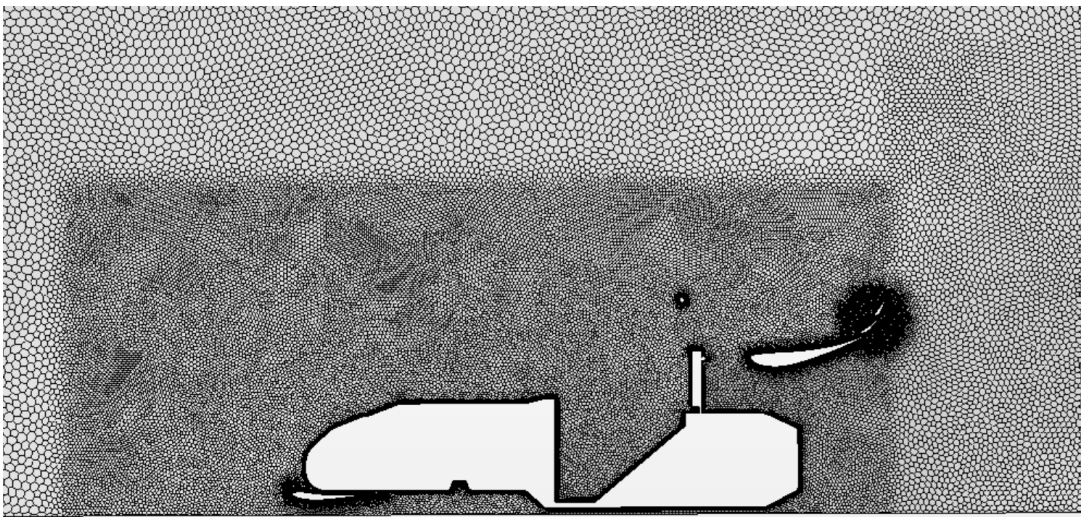

Figure 4.6: Mesh domain: gradient meshing around the car

$$y^+ = \frac{yu_t}{\mu} \tag{4.1}$$

where y is the cell thickness, u_t is friction velocity, and μ is the fluid's kinematic viscosity.
In this case, around 14 prism layers with 3 mm of cell thickness for the first cell (y) and scaled up to a total thickness of 20 mm. Allowing for a fine boundary layer formation over the vehicle's surface and ground simulates the real world case scenario. After all the above steps of meshing over the model, one can see the prism layer formed as shown in Figure 4.7.

Solver CFD numerical simulation using Star CCM+ as a solver is required to be configured to get accurate results. The turbulence model used, boundary conditions applied, and stopping criteria are mentioned in Table 4.2. All the chosen parameters are by considering the best suitability for this application and by referring to the

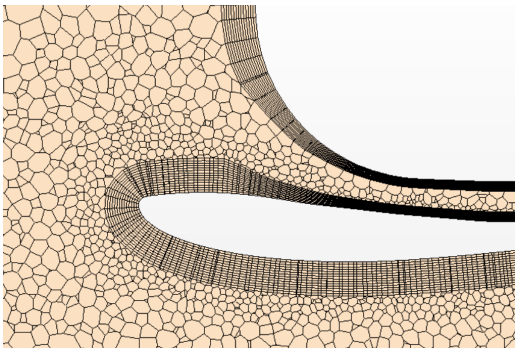

Figure 4.7: Boundary domain: prism layers

previous year's (CFS17) report, the selected speed is $22.22\,\mathrm{m\,s^{-1}}$ or $80\,\mathrm{km\,h^{-1}}$.

4.3 Controller methodology

This section discuss in which ways aero components such as front wing and rear wing flaps are actuated and manipulated by the data from the autonomous system. There are different types of components used, such as servos, sensors and microcontrollers.

4.3.1 Algorithm and components

Input parameters to the system are:

- Yaw rate and yaw angle
- Longitudinal velocity and acceleration
- Lateral velocity and acceleration
- Damper position (compression of spring)
- Steering wheel angle

The basic protocol upon which the actuator (in this case, servos) can be actuated is built by reading the data from the IMU. By considering the particular data and satisfying the conditions, the necessary signal is sent. The servo is attached to flaps in the front wing and rear wing, respectively. Upon receiving the *power width modulation* (PWM) signal from the driver, which is sent by a microcontroller to actuate the servo, the movements of the flaps are achieved.

The servo used is a high torque servo motor with activation angle between 0 to 180° controlled through a PWM signal. The servo driver used is an Adafruit PC9685 capable of controlling up to 16 servos, the driver acts as an intermediate translation part between the servo and microcontroller.

Table 4.2: Solver setting

Simulation		Settings/models
Turbulence model		RANS model
k-epsilon model		RNG k-ϵ
Wall layer		Two layer wall all $y+$ wall treatment
Boundary condition		
Inlet velocity		
Velocity specification method		Magnitude and direction
Velocity magnitude		$80\,\mathrm{km\,h^{-1}}$
Flow direction		along x
Specification method		Intensity and viscosity ratio
Turbulence viscosity ratio		10 %
Turbulence intensity		0.01
Pressure outlet		
Specification method		Intensity and viscosity ratio
Back flow turbulence viscosity ratio		10%
Back flow turbulence intensity		0.01
Reference Values		
Frontal area		$1.09\,\mathrm{m^2}$
Density of air ρ		$1.184\,15\,\mathrm{kg\,m^{-3}}$
Viscosity of air		$1.855 \times 10^{-5}\,\mathrm{Pa\,s}$
Reference volume		Air
Solution methods		
Scheme		Coupled
Space		Three-dimensional
Flow		Coupled
Equation of state		Constant density
Time		Steady
Viscous frame		Turbulent
Stopping criteria	1000+ iteration	mean monitor criteria

The basic algorithm was tested in Matlab as it provides basic functionality to control the servo through an Arduino extension program. The developed code reads the data from the *comma separated value* (CSV) file. This CSV file contains the data read from an actual car driven in numerous circuits, extracted from an optimum G application (A vehicle dynamics software solution that assists us in gathering data from the vehicle's on-board diagnostics.)

For actuation, the longitudinal acceleration data, velocity and the yaw angle of the vehicle with respect to the moving direction is considered. The first condition is to activate the system. To activate the system, the vehicle has to be in a certain speed range because aero vectoring will not make much difference if the velocity is very low, and similarly, if the vehicle velocity is very high, aero vectoring makes the vehicle unstable and may result in unsafe behavior. For the rear wing to actuate the longitudinal acceleration is used. Suppose the longitudinal g is above a certain limit. Accordingly, in that case, a percentage of PWM value is generated and sent to the

Figure 4.8: High torque Servo motor

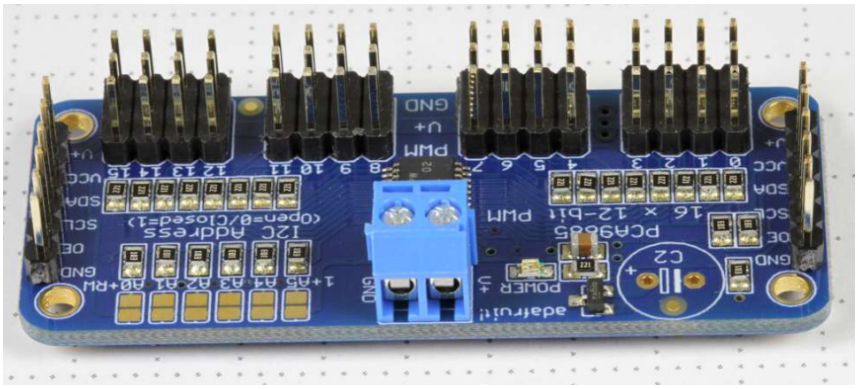

Figure 4.9: The Adafruit PC9685 servo driver

servo, which actuates the flaps in the rear wing. Figure 4.10 shows the difference in flap angles upon activation of the rear wing.

The front wing contains multi segment flaps on both sides, two on the left side and two on the right side. One can actuate the segments on both sides independently. For the actuation of wing flaps, the system reads particular data such as yaw rate (This particular yaw rate is derived from a bespoke two track model built in the one of the microservice in the system). By reading this value, it can determine whether the vehicle is taking a right turn or a left turn, and actuation of either servo 2 (right flaps) or servo 1 (left flaps) is based upon the amount of rotation (yaw rate).

The Figure 4.11 shows the front flap actuated upon receiving the signal. This basic algorithm can then be integrated into the overall control system of the autonomous vehicle. In a microservices based architecture, such as that used in the Lynx car, a microservice is programmed to receive IMU values and speed signals and output the corresponding servo angles, as shown in Figure 4.12.

Figure 4.12 represents the integration between the autonomous system and the active aero system implemented in a microservice based architecture.

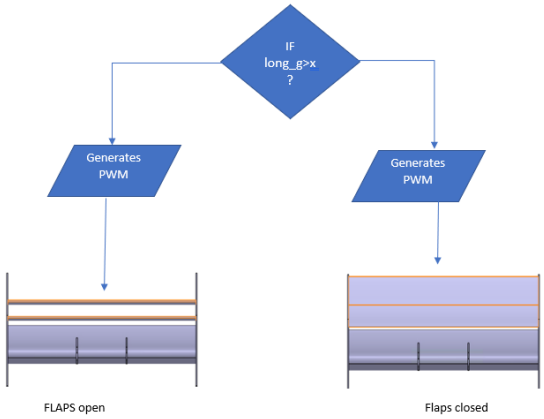

Figure 4.10: Rear wing flaps actuation: like DRS

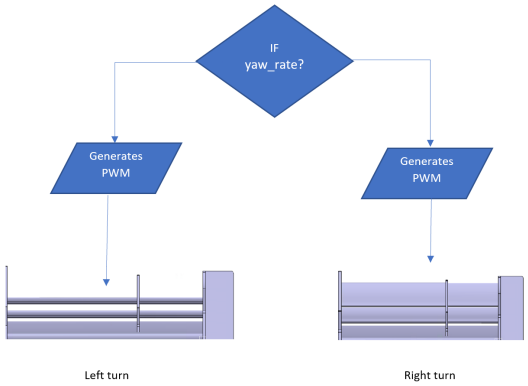

Figure 4.11: Front wing flaps

4.3.2 Flaps mechanism

As previously mentioned, the CFSD21 car has the multi-wing segment aero package. The rear wing has three segments, one being the main base platform and the other two flaps that can be rotated along the Y-axis. Figure 4.13 shows the mechanism used for rotating the flaps of the rear wing. Powered by a single servo with a good actuation angle span, the rear wing can be switched from a high downforce high drag position to a low downforce low drag position with high precision. Also, a servo is tucked inside the end plate, providing almost no adverse effect on the airflow.

The whole linkage mechanism weighs less than 1 kg and can provide good torque to rotate the flaps. Since its PWM servo has a transient angle between fully open and closed flap positions, the wings can have numerous orientations.

The front wing flaps were initially fixed to the side end plates, restricting motion in any axis. With slight modification, it can now accommodate rotation. The mechanism is depicted in Figures 4.14 and 4.15. Both sides of the front wing have the exact same actuation mechanism and control various AOA for flaps. Here the servo and linkages are exposed to the airflow. This will cause some blockage to the flaps and may result in a few counts of drag created by the linkage itself.

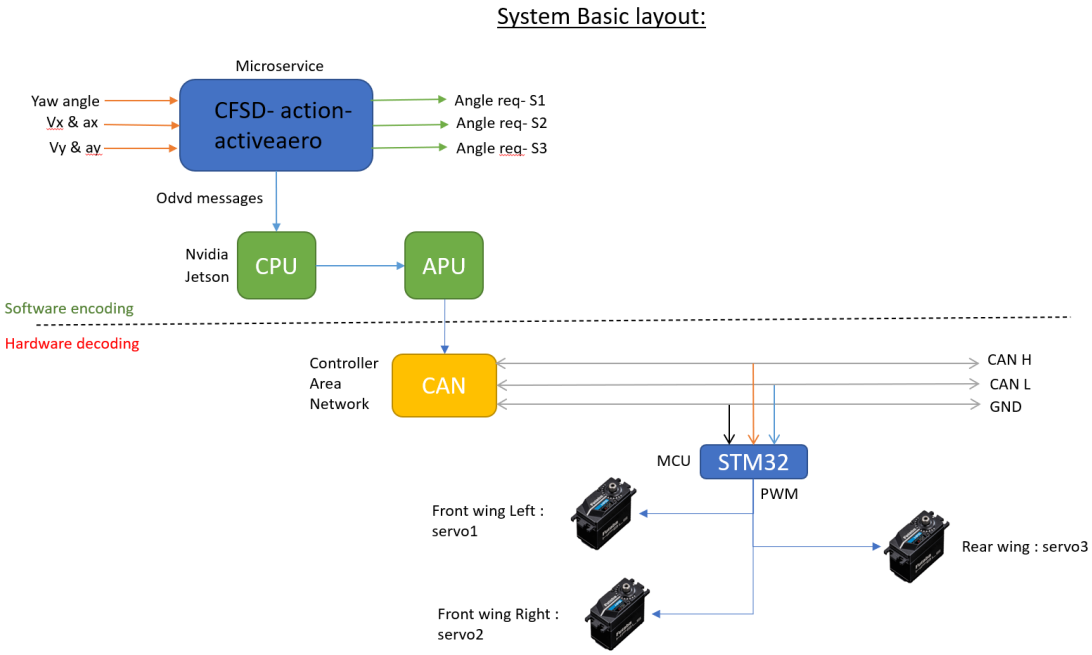

Figure 4.12: System architecture visualised

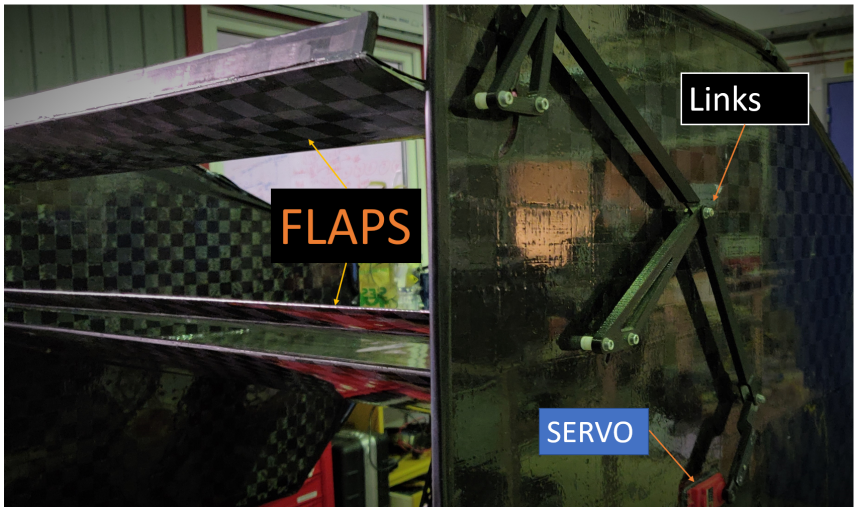

Figure 4.13: Rear wing actuation mechanism (conceptual design)

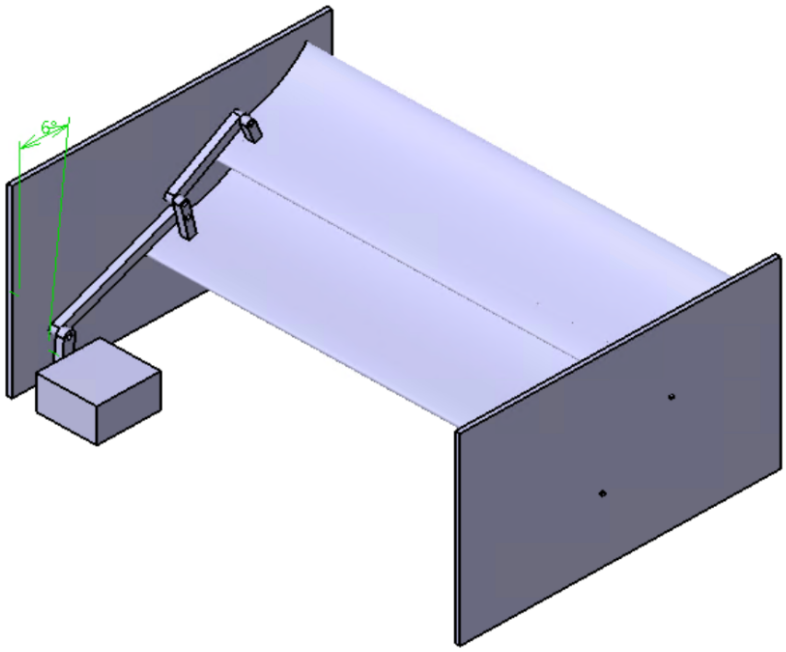

Figure 4.14: CAD concept design: Front wing actuation mechanism

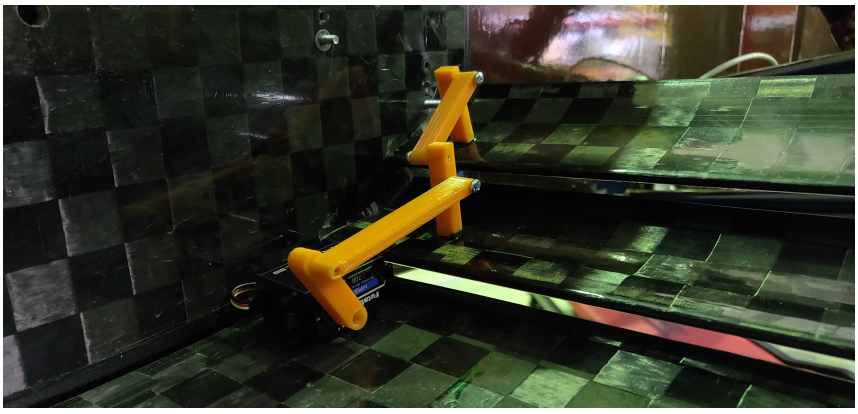

Figure 4.15: Front wing actuation mechanism

5
Results

This section discuss the results obtained through CFD simulation with Star CCM+ for aerodynamics simulation, corresponding to a base model and then the wing actuated setup. Simulation data was compared with the CFS17 results and verified.

5.1 Simulation results

This will be divided into two sections: one observing the car's base model and understanding the flow physics when wings are stationary, and the other determining the drag and lift counts for the base model. The second section includes the results for various configurations of the aero package, like the flow physics when the only rear wing is actuated and only the front wings are actuated. And what will be the effect on drag and lift when both wings are live and actuating at various AOA.

The simulation setup was previously explained in the method part, and the simulations ran 1000+ iterations with conditions such as mean drag and lift coefficient gradient value being less than 0.02 as stopping criteria and the residuals until convergence is achieved.

5.1.1 Simulation results: Base aero package

The base aero package is when all the wing elements are stationary at there highest possible AOA to generate as much downforce as possible.

Static pressure is the pressure at the static part of the body where the amount of force exerted at the surface provides the most resistance to the flow and also where flow becomes stagnant, resulting in drag creation, as the name implies. From Figure 5.1, one can see that the front cone of the monocoque, driver head padding, and rear wing are the major contributors to stagnant pressure (indicated by the slightly dark region in Figure 5.1). In addition, we can see a transient pressure condition over the wheel, where the velocity of air will accelerate compared to the mid surface of the tire. Hence, we see a light blue shade, indicating the pressure gradient at that location.

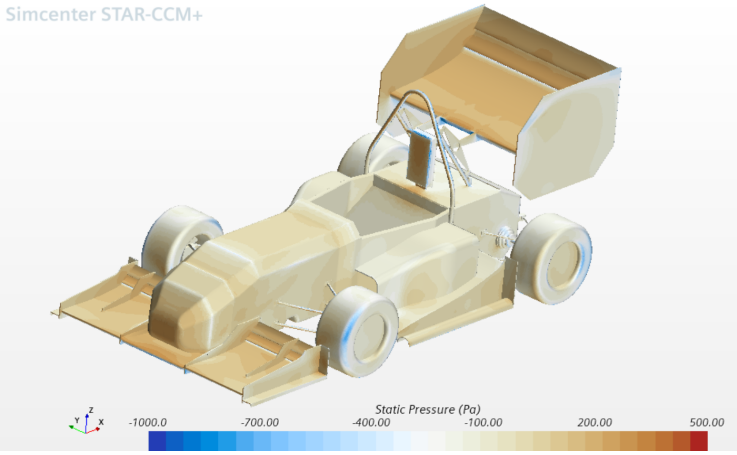

Figure 5.1: Static pressure

Velocity vector field is the velocity vector represents how the air moves over the car's surface with a relative velocity to the surroundings. From Figure 5.2 can observe that with a free stream velocity of $22.22\,\mathrm{m\,s^{-1}}$ or $80\,\mathrm{km\,h^{-1}}$. As the airflow interacts with the car's surface in some places, it decelerates and accelerates in some areas. As previously mentioned, the front cone of the monocoque provides resistance to the flow motion here. One can see that as the velocity of the fluid drops significantly, and in some other sections, such as underneath the front wing, the diffuser and rear wing, can see the accelerated flow velocity. Additionally, some flows are swirling inside the monocoque where the fluid flow is getting tumbled around, generally known as a separation bubble. This is due to the pressure gradient inside the monocoque and outside of it. Hence, flow is getting sucked in and circulated there and causing drag.

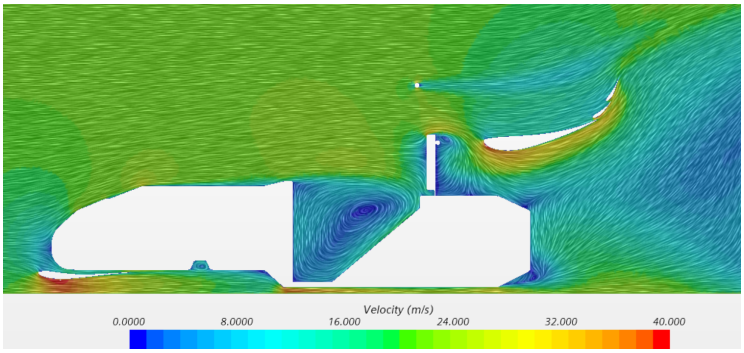

Figure 5.2: Flow velocity around the car

Streamline velocity, the velocity of fluid visualized in terms of lines or packets helps to understand fluid motion across the car's body, as shown in Figure 5.3. This also allows us to identify where exactly the flow is getting turbulent and where and how the vortexes are generated. Turbulence behind the wheel of both axles are

shown in the Figure 5.4.

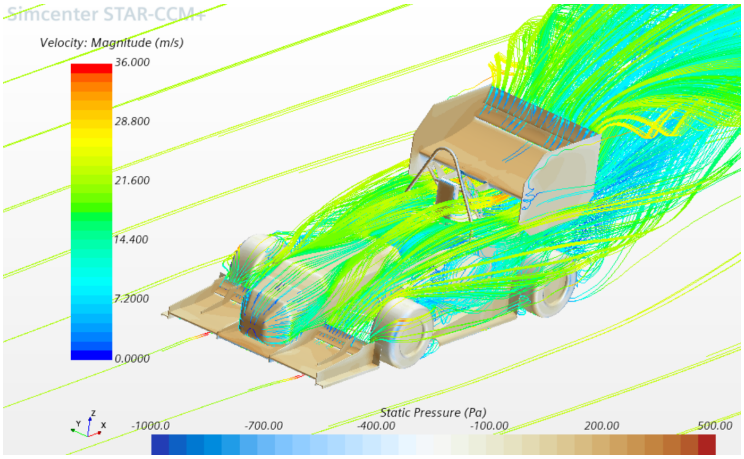

Figure 5.3: Streamline velocity around the car

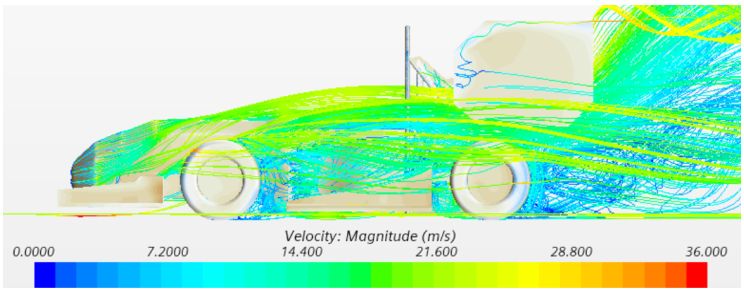

Figure 5.4: Turbulence generated

The vortex is generated at the end plates of the rear wing. This may be accounted for by the pressure difference between both regions, the high pressure flow tends to move towards the low pressure side, creating a vortex as represented in Figure 5.5.

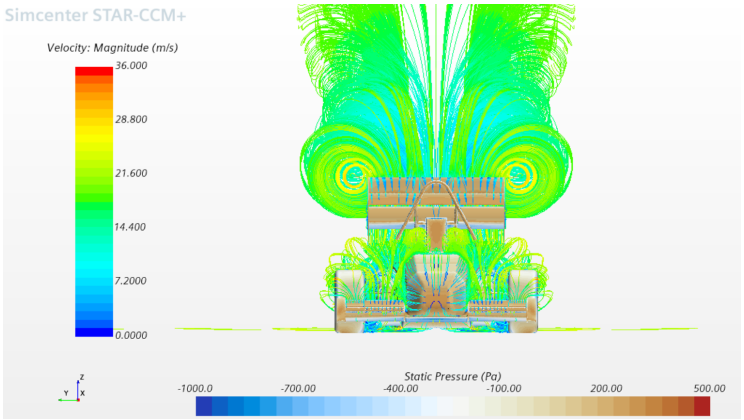

Figure 5.5: Vortex generation

Section-cut pressure and velocity, the positive difference in wind velocity between wing sections (between the top and bottom of the wing) is the sole reason

for creating negative pressure. This negative pressure gradient is attributed to the downforce created. Figure 5.6 shows the pressure concentration at wing segments, visualizing the gradience in pressure distribution where the suction is occurring, resulting in downforce creation. The green part indicates a low-pressure region resulting in suction creation and the red part indicates a high-pressure region.

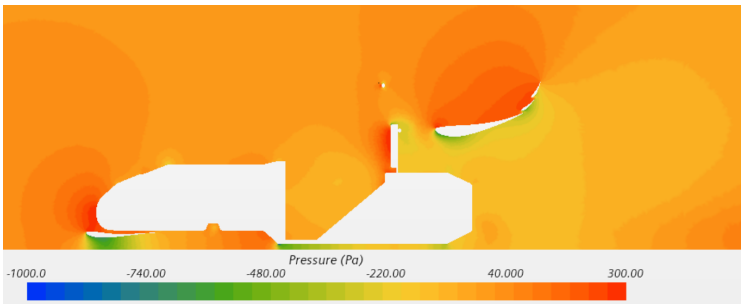

Figure 5.6: Pressure gradient

Similarly, the velocity profile for the wings represents, as previously explained, beneath the front wing, as pressure decreases, the velocity of the fluid increases, creating a venturi effect. Since this setup of the car does not have the diffuser at the end of the body, it loses some of the downforce created. Pockets of low velocity inside the monocoque and on the wake side of the car and behind the headrest padding are indicated by the blue sectors shown in Figure 5.7. Based on the wake scale behind the vehicle body, which will be a comparable term for the upcoming configuration, one can judge how much the rear wing resists the high-velocity fluid flow.

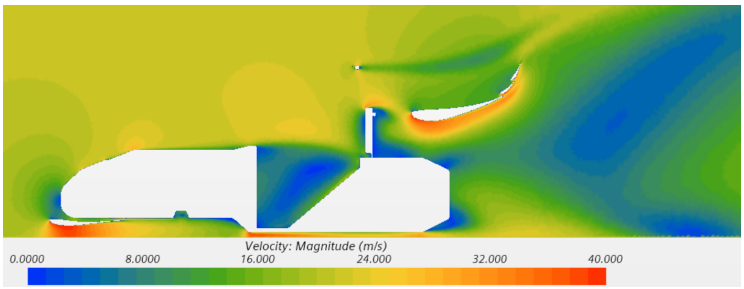

Figure 5.7: Velocity gradient

Numerical results

Drag coefficient is a dimensionless quantity that helps to quantify the amount of resistance offered by the chassis to the fluid motion. From the values, one can see the individual drag contribution by each part of the car's body. The Table 5.1 shows the value of the drag coefficient for every part of the car body.

Table 5.1: Coefficient of drag for various parts of the car.

Part	C_d
Front cone	0.058
Monocoque	0.26
Front wing	0.142
Side pod	0.012
Diffuser	0.087
Rear wing	0.469
Suspension	0.0419
Wheels	0.159
Total	1.22

A significant contributor to the drag is the monocoque and wheels. As illustrated in the above figures, the disturbances and swirls created in and around these parts are a significant source of drag. Similarly, the front wing and rear wing are in the position of high AOA. Hence, the drag created by them is also relatively high (but this is a trade-off for the downforce gained by those parts).

The term "**coefficient of lift**" refers to a dimensionless quantity that helps to quantify the amount of negative lift generated by the chassis in relation to fluid motion. A similar table has been constructed to see the contribution of each part of the chassis to the downforce generated. The Table 5.2 shows the value of the coefficient of lift for every part of the car body.

Table 5.2: Coefficient of lift for various parts of the car

Part	C_l
Front cone	0.058
Monocoque	-0.093
Front wing	-0.388
Side pod	0.039
Diffuser	-0.180
Rear wing	-0.397
Suspension	0.006
Wheels	0.0382
Total	-0.92

A negative value indicates the downforce generated. Here, the major contributors to downforce are the rear and front wing, as this was the main aim of those parts. The diffuser also helps to gain some downforce, but a little lower value is due to the not so fresh air inducted towards it (as shown in Figure 5.4, turbulence in front of the diffuser decreases its efficiency). The interesting part here is the downforce created by the monocoque, as this was intended by the CFS17 team to gain some

negative lift counts (can be seen in the Figure 5.6 as near the diffuser, the chassis develops some suction zone due to the optimized shape of the chassis itself). Furthermore, as can been noted from the difference in sign, the wheels and suspension generates lift.

Total drag force is the amount of force in Newton generated by the chassis equivalent to the above coefficient of drag values. The Table 5.3 shows the value of the total drag force for every part of the car body.

Table 5.3: Total drag force for various parts of the car

Part	Drag [N]
Front cone	9.3
Monocoque	42.1
Front wing	19.7
Side pod	1.95
Diffuser	13.9
Rear wing	75.5
Suspension	6.7
Wheels	25.4
Total	194.5

As predicted from the coefficient of drag values and from the initial assumptions, the rear wing is a significant contributor to the drag. Next comes the monocoque. Wheels are also offering some significant parts of the drag. Therefore, when the car is traveling at 80 km h^{-1}, it has to push through 194.5 N or 20 kg of resistance offered by its chassis to the incoming air. Also, self weight (mass of the car) and this extra load does result in some losses in terms of the energy spent and the velocity the car can achieve.

Total lift force is the amount of force generated by the chassis equivalent to the above discussed coefficient of lift values. The Table 5.4 shows the value of the total drag force for every part of the car body.

Table 5.4: Total lift force for various parts of the car

Part	Lift [N]
Front cone	7.9
Monocoque	-46.7
Front wing	-193.82
Side pod	19.7
Diffuser	-90.04
Rear wing	-198.94
Suspension	3.21
Wheels	19.07
Total	-479.98

Again, negative values indicate downforce from the parts of the chassis. The rear wing and front wing are significant contributors to the downforce. The current base setup car chassis can generate around 480 N or 50 kg of downforce at 80 km h^{-1}. The above results may vary a little depending on the practical, real world values. Due to design constraints and computational cost, the model has been simplified a bit. This may result in a deviation in the values as mentioned. Mesh dependency was also checked with mesh cells ranging from 45 million cells to 15 million cells. The results obtained for both are within a 2 to 5% margin of error; thus, in terms of computational and time constraints, the lower mesh cell model was used to run the simulations.

5.1.2 Simulation results: Actuated wings

The results for various open wing setups will be presented in this section. The first setup is when only the rear wings are opened (dubbed as DRS), the second setup is when only the front wings are opened, and the third setup is when both rear and front wing flaps have been opened. This strategy will depend on how much effect the individual changes are having on drag and lift. The simulation setup is the same as the base setup with the same mesh cells and region boundary. The only thing changed will be the AOA of those wing flaps. By doing so, the meshing layout around the wings will change a bit. Apart from this, it is same as the base simulation setup.

The rear wing flaps are wide open, allowing a passage of air to pass through that gap. By doing so, reduces the stagnant pressure at that location, which could be noted from Figure 5.1 and Figure 5.8, the changes in red region over the rear wing flaps. Thus reducing the drag and downforce significantly.

Static pressure scene from the Figure 5.8, one can see the difference in the static pressure area from the pressure scalar scene, as previously seen in Figure 5.1. The rear wing, since it is open to most of the fluid, has an easy flow out of open flaps, thereby reducing the stagnation of flow fluid at that junction.

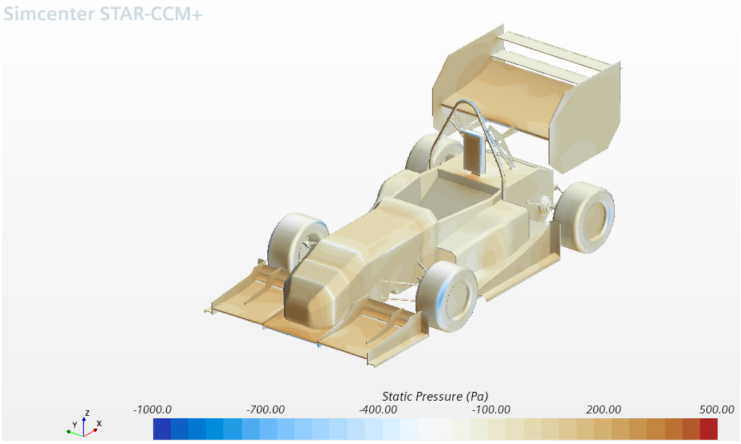

Figure 5.8: static pressure DRS actuated

Then, observing the velocity vector scene in Figure 5.9, shows the difference in the car's wake as there is a smaller zone of lower velocity compared to Figure 5.3. This may be again accounted for an extra passage for fluid flow allowed through rear wing flaps. The open rear wing reduced the wake generated.

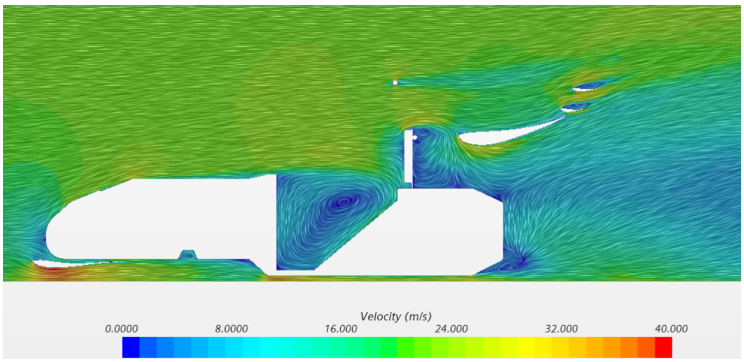

Figure 5.9: Velocity vector for DRS actuated

However, from Figure 5.10, one can observe that there is not that much difference in turbulence created at the rear of the front wheel and the backside of the rear wheel. So one can expect to have a major drag contribution from the wheels again. As expected, the changes made are not related to the flow physics in front of the rear wing section.

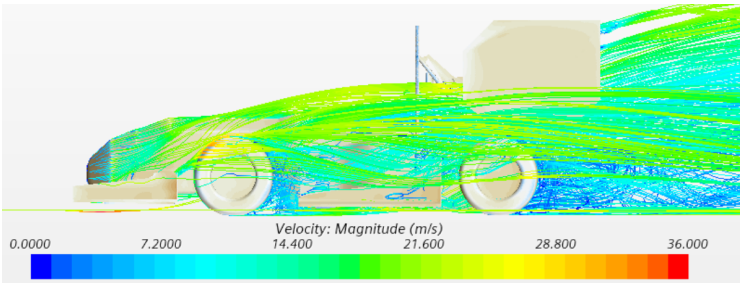

Figure 5.10: stream turbulence near wheels

When observed at the section cut intersection, the major difference in terms of static pressure and velocity of the flow is near the rear wing. One can spot the difference in the static pressure concentration region and in the wake of the car. The wake of the car has been pushed back, accounted by the action of the rear wing, allowing fast flowing air to flow through it. Hence, the wake scale is downsized.

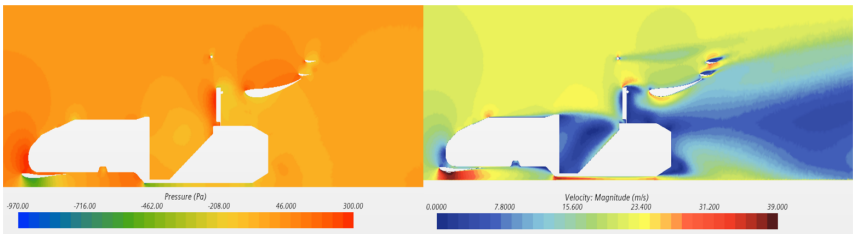

Figure 5.11: Pressure(left) and velocity(right) scene at section plane

Numerical results, drag coefficient values recorded below can see a major difference in drag reduction, as the name suggests DRS. Drag is reduced around 32.9% from the base model, which proves the above images as accurate as possible, where it was observed a reduction in static pressure spots and reduction in wake generated.

Looking at the values between the base and DRS setup, one can see a drastic reduction in rear wing drag count by almost 340 counts (1 count equals 0.0001 of C_d), when compared with the values given in Tables 5.1 and 5.5.

Table 5.5: Drag for various parts of the DRS setup

Part	C_d
Front cone	0.065
Monocoque	0.22
Front wing	0.153
Side pod	0.009
Diffuser	0.073
Rear wing	0.132
Suspension	0.044
Wheels	0.123
Total	0.819

The coefficient of lift is one of the significant factors concerned. In the base setup, high downforce is prioritized over the drag produced by it. Downforce is reduced by 23.9% percent compared to the base setup with this setup. When comparing Figures 5.11 and 5.6, one can see that the low pressure region beneath the rear wing has been drastically reduced. This will decrease the negative lift count as well as the drag.

Table 5.6: Coefficient of lift for various parts of the car

Part	C_l
Front cone	0.016
Monocoque	-0.074
Front wing	-0.365
Side pod	0.038
Diffuser	-0.0137
Rear wing	-0.345
Suspension	0.0063
Wheels	0.0352
Total	-0.70

The total drag force over the car will be reduced, as will the resistance offered by the rear wing to incoming fluid flow. From the tabulated values between Tables 5.3 and 5.7, rear wing drag was reduced by around 61 N. So, the total resistance to the car's longitudinal traverse is reduced.

Table 5.7: Total drag force for various parts of the DRS car

Part	Drag [N]
Front cone	9.05
Monocoque	31.4
Front wing	21.43
Side pod	1.35
Diffuser	10.2
Rear wing	13.86
Suspension	6.2
Wheels	17.16
Total	110.65

The total downforce generated as expected is reduced from the rear wing actuation. The difference in downforce generated by the rear wing is 198 N to 75 N, that is 62% reduction in downforce or that much force exerted vertically on tires is reduced. Can compare the values between the Table 5.8 and 5.4. Reduction in downforce generated will reduce the contact tire patch width and gives less traction, but the purpose of DRS is to use it when the downforce is not a major concern, when speed is. This reduction in drag plays a positive effect on the speed achieved in straights and results in a significant difference in lap timing.

Table 5.8: Total lift force for various parts of the car

Part	Lift [N]
Front cone	8.29
Monocoque	-37
Front wing	-181.92
Side pod	19.3
Diffuser	-68.4
Rear wing	-74.88
Suspension	3.18
Wheels	17.57
Total	-313.86

Front wings actuated, similar to the rear wings. The front wing is a multi element wing package and two flaps on either side of the front wing can be actuated individually. For this section, have combined all the scenes and explain them one after another, and also explain the changes observed.

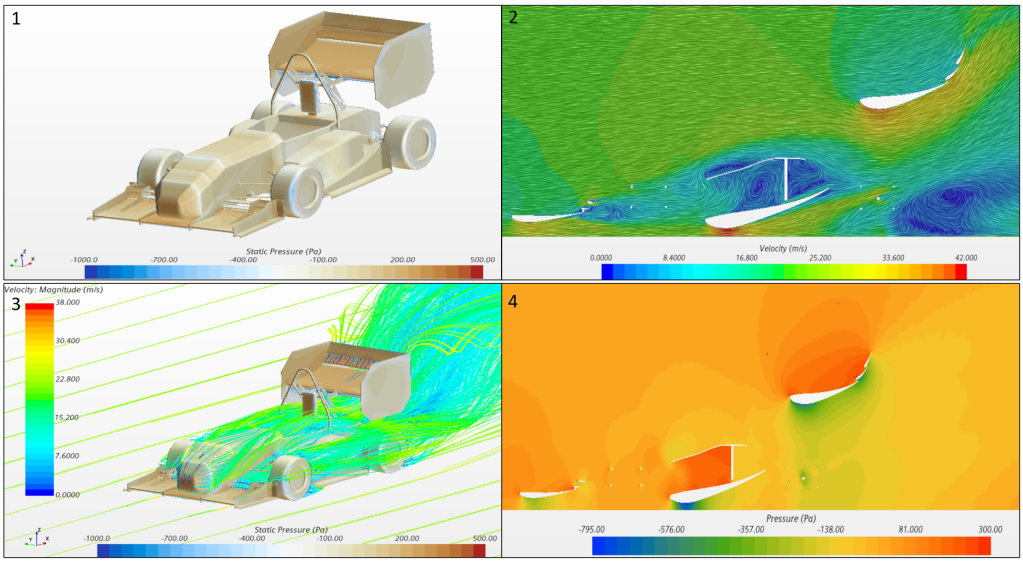

Figure 5.12: Static pressure(Top left panel), Velocity vector(Top right panel), Stream line(Bottom left panel) and pressure cut section(Bottom right panel)

Since the front wing flap area is less prominent than other car chassis parts, it is harder to see the difference right away. For the pressure scene, the difference is hardly noticeable. The velocity vector (the section cut is intentionally taken on the side wing profiles) helps to see a small pocket of fluid flow from the front wing flaps, as shown in Figure 5.13. This will directly affect the turbulence that was observed in the previous setups. Even the section cut pressure scene requires a closer look to note the difference in flow physics for this setup. And the value difference between

drag force and lift force indicates the desired changes.

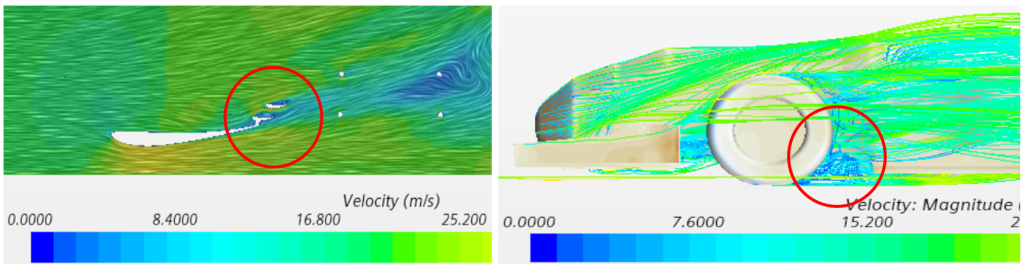

Figure 5.13: A closer look at pressure and turbulence between front wheel and flaps

The role of the front flaps is more in yaw response than in drag reduction, which can be seen in upcoming results. This increases or deducts the load applied by the front wing upon both the left and right tire, which helps in quick directional changes. For this configuration, the coefficient of drag is around 1.19 with a total drag of 190 N. In the case of the co-efficient of lift, it is -0.80 with a downforce of 400 newton.

Complete aero package actuated, The current aero package has six flaps that can be actuated, two from the rear wing and two each from the left and right side of the front wing. This section will observe how the flow physics is altered when all the flaps are in an open position.

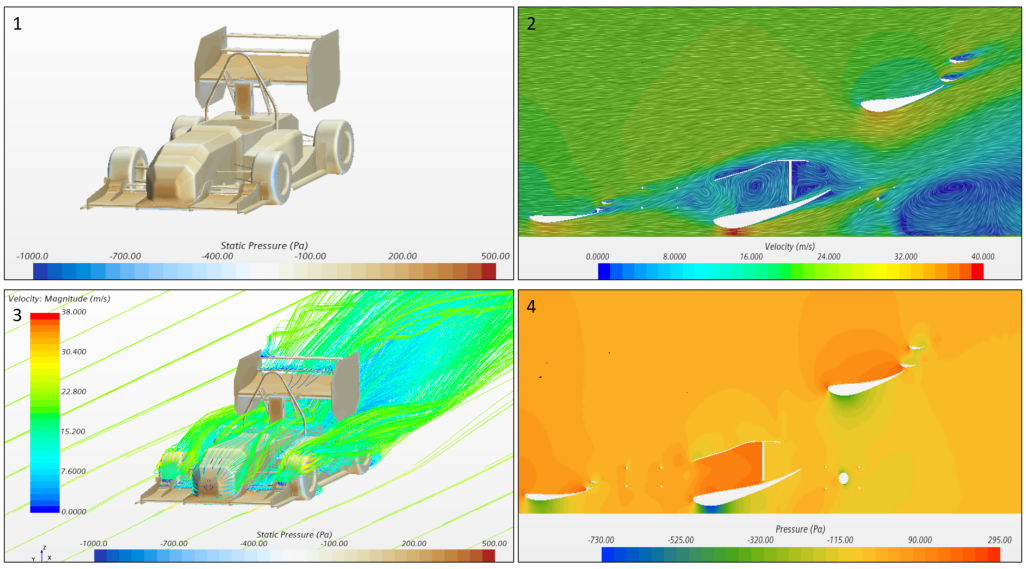

Figure 5.14: Static pressure(Top left panel), Velocity vector(Top right panel), stream line(Bottom left panel) and pressure cut-section(Bottom right panel) for active flaps

From Figure 5.14, note the difference in flow physics and quite different flow field characteristics when compared to the last three setups. Flow physics typically varies for a very slight change in shape and other minute aerodynamic factors. As observed previously, DRS was able to reduce drag and lift. The same goes for the front open wings. But when both are combined, the result will not be the same as predicted because the flow physics may change, as flow that feeds into the front underbelly of the diffuser and rear wing may vary drastically. Hence, the number can't be expected to be added to one another, creating as little drag as possible. The numerical values gives a better idea of the improvements made by the modifications and changes driven by each part. The values are tabulated in the Figure 5.15.

Coefficient of Drag	
Part	Cd
Front cone	0.059
Monocoque	0.249
Front wing	0.0883
Side pod	0.006
Diffuser	0.089
Rear wing	0.140
Suspension	0.044
Wheels	0.129
Total	0.804

Drag forces	
Part	Drag [N]
Front cone	7.72
Monocoque	34.44
Front wing	12.21
Side pod	0.91
Diffuser	12.42
Rear wing	19.52
Suspension	6.17
Wheels	17.99
Total	111.38

Coefficent of Lift	
Part	Cl
Front cone	0.0191
Monocoque	-0.08043
Front wing	-0.234
Side pod	0.0421
Diffuser	-0.163
Rear wing	-0.177
Suspension	0.0041
Wheels	0.0325
Total	-0.55

Lift forces	
Part	Lift [N]
Front cone	9.54
Monocoque	-40.92
Front wing	-112.7
Side pod	21
Diffuser	-81.64
Rear wing	-88.86
Suspension	2.08
Wheels	16.19
Total	275

Figure 5.15: Coefficient of drag, lift and total drag and lift forces tabulated

As previously stated, the coefficient of drag at around 150 counts is less than the DRS configuration and several counts less than the front wing configuration, resulting in a total drag reduction of 35% from the base model. In terms of lift coefficient, it dropped from -0.92 to -0.55. In other words, there is a 40% reduction in downforce when all the flaps are in an open position. The total drag offered by the chassis also dropped from 192 N to 111 N, as shown by the C_d table values in Figure 5.15. The same is true for the negative lift values, reduced from 480 N to 275 N, which releases at least 43% of the vertical load on tires. These results look promising and are heading in the right direction. These minor tweaks may help to reach the maximum speed and maintain high downforce characteristics when required.

6

Discussion

In this section, I will try to cover the consequences of the changes made and their implications in real life. By explaining how it will have an effect on understanding the aerodynamic aspects of the car, as well as the results and conclusion. Also, while doing so, I can address the research questions.

As we saw from the results section, in different setup such as when only front wing, rear wing, and when complete aero package was activated. The aim of reducing the drag and downforce was achieved, with a total of a 35% reduction in drag and a 40% reduction in downforce. Both of these terms will have a direct effect on the top speed, traction, and maneuverability of the car. Since the aim of this project is to have less drag on straights and good efficiency in terms of battery consumption, But, in terms of aero balance and how much of the performance in terms of lap timing is yet to be known, which can only be understood by testing the car on track.

Coming to the answering the research question through results obtained. Until now, all the results obtained and our understanding of the results were only in the simulation. To validate the results obtained, the physical implementation has to be installed on the car. Although simulation is getting as close as possible to the real world, testing the physical car gives a better idea of performance enhancements. The performance of the active aero on the autonomous car looks promising from the results obtained in terms of the virtual figures obtained, and the active system's implementation into the autonomous system blends effectively because all the sensors and hardware required for the active aero system are already in the package.

To know the performance-to-implementation cost ratio, it is yet to be determined through physical testing. The advantages of implementing active aero in an autonomous car are beneficial in terms of efficiency and range by decreasing the drag of the car; in terms of safety as well, this could have a positive impact [15]. The dependency on fluid simulation is getting greater these days because of the close correlation to the real world and because it could control various parameters, although these parameters could be included in the calculation. Still, the cost of computing and time is high. So, a comparatively balanced blend of both physical testing and simulation yields the best results possible. So in the next section, I present the ideas to be implemented for future use, which could be helpful in terms of understanding and improving both the model and results.

6.1 Future work

Improvements could be made to the simplified CAD model. In the current model, I have omitted the suspension uprights, brake assembly, and steering sections. Those parts induce some resistance to the flow and alter the flow fed to the diffuser and side pod. Therefore, these parts can be implemented in further design iterations that will make the model as close to the real car as possible. The results could get better if a test was conducted on the model in a wind tunnel using a scaled model to corelate. This would have helped to get a better idea of the pitch, roll, and lateral movements of the car. Since front wing flaps are comparatively small, the effectiveness of the flaps towards aerovectoring is not that great. As a result, while testing, the driver cannot sense the difference created by the front wing flaps. Hence, backup data from the wind tunnel study is needed to justify the front wing element actuation.

Currently, for the front wings, the servo and links obstruct the flow to the wing by a bit of a margin. The link mechanism can be redesigned to avoid this; one suggestion is to house the servos within the main wing segment by creating a pocket or hollow section. For link struts, placing them close to the endplates will reduce the flow obstruction. The servo and links offer some resistance but can be relatively neglected compared to the other drag producing parts.

Physically testing the car on the track could have helped to note the differences in speed achieved and in terms of lap timing when the aero systems are used. Additionally, load testing the link mechanism could give a better idea of its durability. Then, from this data, it is possible to redesign the structure of the struts or change the material itself.

In addition, repetitive testing can spot flaws in the code or run into an error on the algorithm side. In contrast, testing can help make the necessary changes to the code and enhance the response time. Advanced features like anti-dive during heavy braking, anti-squat during heavy acceleration, and other necessary stability programs that could improve the functionality of the package can be implemented in the future.

7
Conclusion

The objective of the thesis was to implement active wing elements in the current aero package by understanding the current setup and altering the aerodynamic characteristics of the car as required.

The first step was to understand the current aero package, determine its functionality, and understand related results. Through numerical simulation, the desired results from varying the angle of attack saw a decrease in the resistance offered by the car, thus reducing the downforce and drag generated by it. Through simulation, I was able to visualize the flow around the car and understand the functionalities of each component on the car. By activating the wings, it had a positive effect on the drag and lift of the car.

Although the results obtained are still theoretical, they need to be proven on real, physical cars. The real mechanism involved in altering the aero components on the car is installed, but the car has not run with the components active. Since, complete re-construction of car did not happened. So, the validation or correlation of the simulation data is yet to be determined. As per implementing some of these components onto a normal passenger car or an autonomous car in terms of both cost effectiveness and performance, this needs to be established. On paper, it provides positive feedback on performance enhancements, and on that basis, one could determine the cost-benefit of it. Also, through recent years' developments in fluid simulation, simulation data is getting as accurate as real-world conditions, and the differences are in the fine margins or in the meticulousness of the environmental parameters. So one can safely say the difference between simulation and physical testing is gradually decreasing.

In conclusion, the idea of implementing active wing elements into a static aero package to improve its aerodynamic characteristics holds true in theory but has yet to be proven in a physical Formula Student car.

Bibliography

[1] Ruqiong Qin and Chunyi Duan. *The principle and applications of Bernoulli equation.* 2017.

[2] James Patrick Merkel. *Development of multi element active aerodynamics for the formula SAE car.* 2013.

[3] Xin Zhang, Willem Toet and Jonathan Zerihan. *Ground effect aerodynamics of race cars, Applied Mechanics Reviews.* 2006.

[4] Milliken, W.F. *Race Car Vehicle Dynamics, SAE International.* 1994.

[5] Andrea Quintarelli. *Aerodynamic efficiency, balance and center of pressure.* 2012.

[6] Jean-Franc, Ois Beaudoin and Jean-Luc Aider. *Drag and lift reduction of a 3D bluff body using flaps.* 2008.

[7] Ahmed SR. *Influence of Base Slant on the Wake Structure and Drag of Road Vehicles.* 1983.

[8] Yuping He. *Design of an Actively Controlled Aerodynamic Wing to Increase High-Speed Vehicle Safety.* 2013.

[9] Simon McBeath. *Competition Car Aerodynamics: A Practical Handbook.* 1997.

[10] MatteoCorno, Stefano Bottelli, Mara Tanelli, Cristiano Spel, Sergio M. Savares. *Active Control of Aerodynamic Surfaces for Ride Control in Sport Vehicles.* 2014.

[11] M.Corno, S.Bottelli, G.Panzani, M.Tanelli, C.Spelta, S.M. Savaresi. *Improving High Speed Road-Holding Using Actively Controlled Aerodynamic Surfaces.* 2013.

[12] Arvin R, Savkoor and C.T, Chou. *Application of Aerodynamic Actuators to Improve Vehicle Handling.* 1999.

[13] Mohammed Hammad, Khizar Qureshi, Yuping He. *Safety and Lateral Dynamics Improvement of a Race Car Using Active Rear Wing Control.* 2019.

[14] Fereydoon Diba , Ahmad Barari , Ebrahim Esmailzadeh. *Active Aerodynamic System to Improve the Safety and Handling of Race Cars in Lane Change and Wet Road Maneuvers.* 2012.

[15] Yuping He. *Design of an Actively Controlled Aerodynamic Wing to Increase High-Speed Vehicle Safety.* 2013.

[16] Lee Wen Yew, Abdulkareem Sh. Mahdi Al-Obaidi, Satesh Narayana Namasivayam. *Design and Development of a Multi-Element Active Aerodynamic Package to Enhance the Performance of Taylor's Formula SAE Car.* 2017.

[17] Krzysztof Kurec, Michab Remer, Jakub Broniszewski, PrzemysBaw Bibik, Sylwester Tudruj, and Janusz Piechna. *Advanced Modeling and Simulation of Vehicle Active Aerodynamic Safety.* 2019.

[18] John D. Anderson, Gerard Degrez, Joris Degroote, Erik Dick, Roger Grundmann and Jan Vierendeels . *Compuational Fluid dynamics An introduction*, pages 5-10. 2009.

[19] Kim, T, Cao, D. *The Steady Navier-Stokes System. In: Equations of Motion for Incompressible Viscous Fluids.*, pages 83-108. 2021.

[20] Michel Rieutord. *Fluid dynamics.* 2015.

[21] Sadrehaghighi, Ideen. *Mesh Generation in CFD.* 2020.

[22] Bengt Jacobson. *Vehicle Dynamics Compendium* 2019.

Department of Mechanics and Maritime Sciences
CHALMERS UNIVERSITY OF TECHNOLOGY
Göteborg, Sweden 2023
www.chalmers.se

CHALMERS
UNIVERSITY OF TECHNOLOGY